

AEDC-TR-73-94

cp. 2

JUL 15 1973
AUG 23 1973
MAR 22 1977
MAY 25 1966
JUL 9 1991
FEB 17 1985



AN INVESTIGATION OF STRAIN WAVE PROPAGATION IN METALLIC CONICAL RODS

J. P. Billingsley, P. A. Evans, and R. L. Nenninger

ARO, Inc.

June 1973

Approved for public release; distribution unlimited.

TECHNICAL REPORTS
THIS COPY

**VON KÁRMÁN GAS DYNAMICS FACILITY
ARNOLD ENGINEERING DEVELOPMENT CENTER
AIR FORCE SYSTEMS COMMAND
ARNOLD AIR FORCE STATION, TENNESSEE**

NOTICES

When U. S. Government drawings specifications, or other data are used for any purpose other than a definitely related Government procurement operation, the Government thereby incurs no responsibility nor any obligation whatsoever, and the fact that the Government may have formulated, furnished, or in any way supplied the said drawings, specifications, or other data, is not to be regarded by implication or otherwise, or in any manner licensing the holder or any other person or corporation, or conveying any rights or permission to manufacture, use, or sell any patented invention that may in any way be related thereto.

Qualified users may obtain copies of this report from the Defense Documentation Center.

References to named commercial products in this report are not to be considered in any sense as an endorsement of the product by the United States Air Force or the Government.

AN INVESTIGATION OF STRAIN WAVE PROPAGATION
IN METALLIC CONICAL RODS

J. P. Billingsley, P. A. Evans, and R. L. Neminger
ARO, Inc.

Approved for public release; distribution unlimited.

FOREWORD

The work reported herein was conducted at Arnold Engineering Development Center (AEDC), Air Force Systems Command (AFSC), under Program Element 65802F.

The results of research presented were obtained by ARO, Inc., (a subsidiary of Sverdrup & Parcel and Associates, Inc.), contract operator of AEDC, AFSC, Arnold Air Force Station, Tennessee. The research was conducted intermittently from January 1968 until July 1972, under ARO Project Numbers VT0878, VT2914 and VG5118. The manuscript was submitted for publication on April 11, 1973.

The authors wish to express their appreciation to personnel of the von Kármán Gas Dynamics Facility (VKF) who helped obtain the experimental data necessary for completion of the research reported herein. Without the able assistance of R. P. Young, K. Sloan, R. R. Jernigan, and their staffs, this report would not have been possible. The encouragement and suggestions offered by J. R. DeWitt, A. J. Cable, G. D. Norfleet and J. L. Potter were particularly helpful. Since a major portion of the enclosed work represents a combination of two theses presented to the University of Tennessee Space Institute in partial fulfillment of the requirements for the Master of Science Degree, the authors gratefully acknowledge the valuable counsel of Dr. M. K. Newman, Professor of Mechanical Engineering. The second author, P. A. Evans, formerly an engineer in the Aerospace Division of VKF, is currently with TVA in Knoxville. The third author, Captain R. L. Nenninger, is deceased.

This technical report has been reviewed and is approved.

JIMMY W. MULLINS
Lt Colonel, USAF
Chief Air Force Test Director, VKF
Directorate of Test

A. L. COAPMAN
Colonel, USAF
Director of Test

ABSTRACT

Strain wave propagation in metal cones with a compressive pulse applied at the base has been investigated experimentally and theoretically. This study was motivated by the need for design information for gun-launched models used in aerophysics research. The results are also directly applicable to the design of ordinary gun-launched munitions or to any other cases of impulsive loading on conical bars. The effect of the following parameters was considered: (1) cone angle, (2) cone tip joint (threaded connection), and (3) cone tip material variation (7075-T6 base with 7075-T6, beryllium-copper, and Fansteel 60® tips). Transient strains were measured with strain gages mounted at critical locations on the specimen. It was found that increasing the cone half-angle from 2 to 10 deg reduced the level of strain amplification for both solid and jointed cones. The effect of a threaded junction between the model base and the tip is to increase the strain (or stress) level in the exterior section because of (1) cross-sectional area decrease at the bottom of the threaded hole and (2) reflected strain from the visible tip junction. Tips of heavier, denser material than the base further intensified the strain in the exterior threaded section because of greatly increased strain reflection at the forward junction. The measured strain amplification at the cone surface was compared with predictions based on one-dimensional strain propagation theory. In general, the theoretical predictions were good enough for use (with reasonable discretion) in model designs.

CONTENTS

	<u>Page</u>
ABSTRACT	iii
NOMENCLATURE	viii
I. INTRODUCTION	1
II. THEORETICAL ANALYSIS	
2.1 One-Dimensional Wave Propagation in a Solid Conical Rod	2
2.2 Wave Propagation in a Bimetallic Conical Bar with Threaded Joints	6
III. EXPERIMENTAL PROGRAM	
3.1 Scope of Investigation	10
3.2 Test Apparatus	10
3.3 Experimental Procedure	13
3.4 Data Reduction Procedure	14
3.5 Error Analysis	15
IV. DISCUSSION OF RESULTS	
4.1 Solid Cones	16
4.2 Jointed Cones	19
V. CONCLUSIONS	21
REFERENCES	23

APPENDIXES

I. ILLUSTRATIONS

Figure

1. A Typical 5-deg Semi-Angle Cone Model and Sabot	29
2. Gun-Launched Model with Bent Nose Tip	30
3. Sketch of Analytical Models	
a. Solid Cone Geometry	31
b. Jointed Cone Geometry (Tip Attachment Angle Is 90 deg to X-Axis)	31
4. Schematic Representation of Strain Impulse Applied to Base of Cone	32

<u>Figure</u>	<u>Page</u>
5. Discontinuity Schematic	32
6. Dimensions of the Solid Cone Specimens	33
7. Jointed Cone Specimen Dimensions and Strain-Gage Locations	34
8. Section View of Air Gun with Test Bar Installed in Firing Position	35
9. Typical Bridge Circuit for Measuring and Recording Transient Strains	36
10. Detail of Test Cylinder Showing Gage Location and Orientation	37
11. Strain Pulse Applied to Base of 2-deg Semi-Angle Solid Cone	38
12. Experimental and Theoretical Strain at Gage No. 8 (10.05 in. from Cone Base) for 2-deg Semi-Angle Solid Cone	39
13. Longitudinal Strain, as a Function of Time, Measured on the 2-deg Semi-Angle Solid Cone as the Wave Propagated from the Base to the Apex	40
14. Longitudinal Strain, as a Function of Time, Measured on the 5-deg Semi-Angle Solid Cone as the Wave Propagated from the Base to the Apex	41
15. Longitudinal Strain, as a Function of Time, Measured on the 7.5-deg Semi-Angle Solid Cone as the Wave Propagated from the Base to the Apex	42
16. Longitudinal Strain, as a Function of Time, Measured on the 10-deg Semi-Angle Solid Cone as the Wave Propagated from the Base to the Apex	43
17. Comparison of Theoretical with Experimentally Determined Strain Amplification in a 2-deg Semi-Angle Solid Cone	44
18. Comparison of Theoretical with Experimentally Determined Strain Amplification in a 5-deg Semi-Angle Solid Cone	45

<u>Figure</u>	<u>Page</u>
19. Comparison of Theoretical with Experimentally Determined Strain Amplification in a 7.5-deg Semi-Angle Solid Cone	46
20. Comparison of Theoretical with Experimentally Determined Strain Amplification in a 10-deg Semi-Angle Solid Cone	47
21. Theoretical and Experimental Strain Amplification in a Jointed 2-deg Semi-Angle Cone, 90-deg Attachment Angle, 7075-T6 Tip	48
22. Theoretical and Experimental Strain Amplification in a Bimetallic 2-deg Semi-Angle Cone, 90-deg Attachment Angle, Beryllium-Copper Tip	49
23. Theoretical and Experimental Strain Amplification in a Bimetallic 2-deg Semi-Angle Cone, 90-deg Attachment Angle, Fansteel 60 Tip	50
24. Theoretical and Experimental Strain Amplification in a Bimetallic 10-deg Semi-Angle Cone, 90-deg Attachment Angle, Beryllium-Copper Tip	51
25. Theoretical and Experimental Strain Amplification in a Bimetallic 10-deg Semi-Angle Cone, 90-deg Attachment Angle, Fansteel 60 Tip	52
26. Typical Permanent Distortion at 45-deg Tip Joint	53

II. TABLES

I. Material Properties of Specimens	54
II. Strain Transmission and Reflectivity Parameters at x_1	54
III. Strain Transmission and Reflectivity Parameters at x_2	54
IV. Cross-Sectional Dimensions and Area Ratios for Solid and Jointed Cone Specimens	55
V. Strain Amplification Factors from Donnell's Analysis for 2-deg Semi-Angle Cones	56

II. TABLES (Continued)

	<u>Page</u>
VI. Strain Amplification Factors from Donnell's Analysis for 10-deg Semi-Angle Cones	57
VII. Strain Amplification Factors from the Combined Fourier-Donnell Analysis for 2-deg Semi-Angle Cones	58
VIII. Strain Amplification Factors from the Combined Fourier-Donnell Analysis for 10-deg Semi-Angle Cones	59

NOMENCLATURE

A_{base}	Base area of cone, $\pi d_b^2/4$, in. ²
A_n	The n^{th} Fourier cosine series coefficient, $\left[\frac{1}{t_1} \int_0^{t_1} \epsilon_{base}(t) \cos \left(\frac{n\pi t}{t_1} \right) dt \right]$
A_0	Fourier series coefficient, $\frac{1}{t_1} \int_0^{t_1} \epsilon_{base}(t) dt$
A_t	Thread cross-sectional area, $\pi d_t^2/4$, in. ²
A_x	Cross-sectional area of cone at x, $\pi d_x^2/4$, in. ²
A_{xeff}	Effective cross-sectional area in the threaded section, $A_x - A_t$, in. ²
a	Theoretical length of cone along the centerline, in. (Fig. 3)
B_n	The n^{th} Fourier sine series coefficient, $\left[\frac{1}{t_1} \int_0^{t_1} \epsilon_{base}(t) \sin \left(\frac{n\pi t}{t_1} \right) dt \right]$

\bar{C}	Strain wave propagation velocity, $\sqrt{\frac{E}{\rho}}$, in./ μ sec or ft/sec
C_n	$\pi n/t_1$
C. A. F.	Compressive strain amplification factor, $\epsilon_x/\epsilon_{\text{base}}$
d_b	Diameter of cone base, in.
d_t	Diameter of thread, 0.212 in.
d_x	Diameter of cone at x, in.
d_1, d_2	Diameter of cone at x_1 and x_2 , in.
E	Material modulus of elasticity, lb/in. ²
$e_A, e_B,$ $e_{\text{in}}, e_{\text{out}}$	Strain-gage circuit voltages (Fig. 9), v
K	Constant of integration defined by Eq. (14)
L	True length of cone, in.
L_{cyl}	Length of cylindrical portion of specimen, in.
r_{AB}	Reflectivity coefficient defined by Eq. (21)
t	Time, sec or μ sec
t_1	a/\bar{C} , sec or μ sec
u	Particle displacement, in.
v	Variable defined by $\bar{C}t - x$, in.
w	Specific weight of material, lb/ft ³
x	Position coordinate, measured from cone base (Fig. 3), in.
x_1	Location of first discontinuity at bottom of thread hole, in.
x_2	Location of discontinuity at cone tip junction, in.
ϵ	$\epsilon(t, x) = -\frac{\partial u}{\partial x}$, strain, μ in./in.
ϵ_{base}	$\epsilon(t)$ = strain applied to base of cone, μ in./in.
ϵ_x	Maximum compressive strain at x, μ in./in.
$\epsilon_{1\text{trans}}$	Strain transmitted across discontinuity at Station x_1 , μ in./in.
$\epsilon_{2\text{refl}}$	Strain reflected at x_2 , μ in./in.

$\epsilon_{x_{refl}}$	Strain in threaded section reflected from x_2 (Eq. (24))
$\frac{\epsilon_x}{\epsilon_{base}}$	Ratio of maximum compressive strain at x to maximum compressive strain applied to the base, C. A. F.
θ	Cone tip half-angle (Fig. 3), deg
ρ	Mass density of material, lb-sec ² /ft ⁴
σ	Longitudinal stress (Eq. (4)), lb/in. ²
ϕ	Arbitrary function of $\bar{C}t - x$ (see Eq. (3))
ψ	Arbitrary function of $\bar{C}t + x$ (see Eq. (3))

SECTION I INTRODUCTION

Light gas gun technology has been developed to the point where certain sabot-model combinations can be accelerated to extremely high velocities (Ref. 1). As a result of aerophysics research programs, small conical models as illustrated in Fig. 1 (Appendix I) are often launched from light gas guns into free flight aeroballistic ranges. The models are subjected to high level impulsive loads on their base during the initial phases of the gun launch cycle.

Typical muzzle velocity for a conical model is up to 20,000 ft/sec. Any permanent deformation of the model caused by the launch cycle can adversely affect model dynamics and invalidate the test data. Large plastic deformations have been observed in photographs of models in free flight (Fig. 2). Joint upset, tip bending, and tip fracture have been the predominant type of failure.

It is evident, then, that the launch cycle stresses on the model-sabot combination must be kept below the elastic limit of the material (Ref. 2). Because of the highly transient nature of the initially applied stresses, the effects of stresses that are applied for a very short time and propagate very rapidly must be considered. In other words, the model designer must be concerned with the effects of stress and strain wave propagation in conical projectiles.

An experimental program was initiated to study the effects of strain-stress wave propagation in single and bimetal cones that were designed and fabricated similar to the conical models used in hypervelocity aeroballistic range work (Refs. 3 and 4). Stress-strain pulses were input to the base of conical specimens, which were machined on the end of a cylindrical rod.

Specifically, such parameters as cone angle, with and without a jointed tip, and tip material were systematically varied and their effect recorded. Electric resistance strain gages were used to record transient strains at strategic external locations on the test specimen. The experimental equipment and procedure will be described in detail later. Experimental data are compared with theoretical predictions where it is feasible to do so.

There is a voluminous amount of literature associated with stress wave propagation in solid cylindrical rods. In contrast, information concerning stress propagation in conical rods has been rather limited. The earliest work on this subject is apparently that of Landon and Quinney which was done during World War I (Ref. 5), and the next investigator was Donnell about 10 years later (Ref. 6).

Interest in stress wave propagation for cones then lay dormant for about twenty years until Kolsky (Ref. 7) commented on the earlier works and presented additional experimental evidence of the peculiar stress wave phenomena associated with cones. Within the last decade interest in conical stress wave behavior has been rekindled. Some theoretical results of recent origin are contained in Refs. 8, 9, and 10. Experimental results are reported in Refs. 11, 12, 13, 14, and 15.

The work reported in Ref. 12 closely parallels some of the results for single-material solid cones that were found early in the present investigation (Ref. 3). Recent theoretical and experimental results presented in Ref. 14 may be applied to the analysis of cones with various discontinuities, including tip joints.

SECTION II THEORETICAL ANALYSIS

2.1 ONE-DIMENSIONAL WAVE PROPAGATION IN A SOLID CONICAL ROD

The following theory for one dimensional wave propagation in conical bars is similar to that mentioned in Refs. 5, 6, and 7. Consider a solid cone as shown in Fig. 3a with impulse strain, $\epsilon(t)$, uniformly applied at the base. The wave caused by the impulse load propagates in a direction of increasing x . For small cone angles, it is assumed that no wave reflections occur at the lateral surfaces of the cone and that there is no variation of the strain in a cross section perpendicular to the direction of propagation. By considering an element at a distance x from the base with thickness dx , the equation of motion for equilibrium of the element may be written as follows:

$$\frac{\partial^2 u}{\partial t^2} = C^2 \frac{\partial^2 u}{\partial x^2} - \frac{2}{(a-x)} \frac{\partial u}{\partial x} \quad (1)$$

where \bar{C} is the velocity with which a wave propagates along a rod and is defined as

$$\bar{C} = \sqrt{\frac{E}{\rho}} \quad (2)$$

Equation (1) is a spherical wave equation whose general solution is

$$u = \frac{\phi(\bar{C}t - x) + \psi(\bar{C}t + x)}{[1 - (x/a)]} \quad (3)$$

where $\phi(\bar{C}t - x)$ and $\psi(\bar{C}t + x)$ represent waves traveling in opposite directions and ϕ and ψ are arbitrary functions which must fit the conditions that pertain to the solution of the problem. Since a plane elastic wave with no variation in strain in the radial and tangential direction of the cone element is being considered, Hooke's law may be used for the stresses at any location as

$$\sigma = E \frac{\partial u}{\partial x} \quad (4)$$

Consider the wave propagating in the direction of increasing x represented by

$$u = \frac{\phi(\bar{C}t - x)}{(1 - x/a)} \quad ; \quad \psi = 0 \quad (5)$$

The compressive strain is given as

$$-\frac{\partial u}{\partial x} = -\frac{\phi(\bar{C}t - x)}{a(1 - x/a)^2} + \frac{\phi'(\bar{C}t - x)}{(1 - x/a)} \quad (6)$$

where

$$\phi'(\bar{C}t - x) = \frac{d\phi(\bar{C}t - x)}{d(\bar{C}t - x)} \quad (7)$$

Equation (6) gives the relationship necessary to calculate the strain at any location (x) and time (t) provided $\phi(\bar{C}t - x)$ is known. Therefore, the strain at some particular time and location is required to solve the equation. For the impulse load applied at the cone base ($x=0$), a rather

general relationship for the strain as a result of the applied impulse force may be defined in the form of a Fourier series as

$$-\epsilon_{base} = \left| \frac{\partial u}{\partial x} \right|_{x=0} = \frac{A_o}{2} + \sum_{n=1}^n [A_n \text{Cos}(C_n t) + B_n \text{Sin}(C_n t)] \quad (8)$$

It may be schematically represented as shown in Fig. 4. The boundary conditions at $x = 0$ are

$$\frac{\partial u}{\partial x} = 0 \quad ; \quad t = 0 \quad (9)$$

$$\frac{\partial u}{\partial x} = -\epsilon(t) \quad ; \quad 0 \leq t \leq t_1 \quad (10)$$

By letting $v = \bar{C}t - x$ and equating Eq. (6) with Eq. (8), an expression for $\phi(v)$ for the case at $x = 0$ may be obtained:

$$-\frac{\partial u}{\partial x} = \phi'(v) - \frac{1}{a} \phi(v) = \frac{A_o}{2} + \sum_{n=1}^n \left[A_n \text{Cos} \left(\frac{C_n}{\bar{C}} v \right) + B_n \text{Sin} \left(\frac{C_n}{\bar{C}} v \right) \right] \quad (11)$$

Since at $x = 0$, v is a function of t alone, the general solution to Eq. (11) is given as follows:

$$\phi(v)e^{-\int dv/a} = \int e^{-dv/a} \left\{ \frac{A_o}{2} + \sum_{n=1}^n \left[A_n \text{Cos} \left(\frac{C_n}{\bar{C}} v \right) + B_n \text{Sin} \left(\frac{C_n}{\bar{C}} v \right) \right] \right\} dv - K \quad (12)$$

where K is a constant of integration.

Equation (12) yields an expression for $\phi(v)$, which is given as

$$\begin{aligned} \phi(v) = & K e^{v/a} - \frac{A_o}{2} a - \sum_{n=1}^n \left\{ \frac{A_n}{(1/a)^2 + \left(\frac{C_n}{\bar{C}}\right)^2} \left[\frac{1}{a} \text{Cos} \left(\frac{C_n}{\bar{C}} v \right) - \frac{C_n}{\bar{C}} \text{Sin} \left(\frac{C_n}{\bar{C}} v \right) \right] \right. \\ & \left. + \frac{B_n}{(1/a)^2 + \left(\frac{C_n}{\bar{C}}\right)^2} \left[\frac{1}{a} \text{Sin} \left(\frac{C_n}{\bar{C}} v \right) + \frac{C_n}{\bar{C}} \text{Cos} \left(\frac{C_n}{\bar{C}} v \right) \right] \right\} \end{aligned} \quad (13)$$

By substituting Eq. (13) for $\phi(v)$ into Eq. (5) for the displacement (u) and applying the initial condition that there is no displacement at $x = 0$ when $t = 0$, the constant of integration (K) may be obtained:

$$K = \frac{A_o a}{2} + \sum_{n=1}^n \left[\frac{A_n/a + B_n C_n/\bar{C}}{(1/a)^2 + (C_n/\bar{C})^2} \right] \tag{14}$$

With the determination of (K), the expression for $\phi(v)$ is fully defined. Substituting $\phi(v)$ and its derivative into Eq. (6) yields the expression for the strain, which may be written as follows:

$$\frac{\partial u}{\partial x} = \frac{1}{a(1-x/a)^2} \left\{ \begin{aligned} & \frac{A_o a}{2} (e^{v/a-1}) + e^{v/a} \sum_{n=1}^n \left[\frac{A_n/a + B_n C_n/\bar{C}}{(1/a)^2 + (C_n/\bar{C})^2} \right] \\ & - \sum_{n=1}^n \left\{ \frac{A_n}{(1/a)^2 + (C_n/\bar{C})^2} \left[\frac{1}{a} \text{Cos} \left(\frac{C_n}{\bar{C}} v \right) - \frac{C_n}{\bar{C}} \text{Sin} \left(\frac{C_n}{\bar{C}} v \right) \right] \right\} \\ & + \frac{B_n}{(1/a)^2 + (C_n/\bar{C})^2} \left[\frac{1}{a} \text{Sin} \left(\frac{C_n}{\bar{C}} v \right) + \frac{C_n}{\bar{C}} \text{Cos} \left(\frac{C_n}{\bar{C}} v \right) \right] \right\} \end{aligned} \right. \tag{15}$$

$$- \frac{1}{a(1-x/a)} \left\{ \begin{aligned} & e^{v/a} \left\{ \frac{A_o a}{2} + \sum_{n=1}^n \left[\frac{A_n/a + B_n C_n/\bar{C}}{(1/a)^2 + (C_n/\bar{C})^2} \right] \right\} \\ & + (a/\bar{C}) \sum_{n=1}^n \left\{ \frac{A_n C_n}{(1/a)^2 + (C_n/\bar{C})^2} \left[\frac{1}{a} \text{Sin} \left(\frac{C_n}{\bar{C}} v \right) + \frac{C_n}{\bar{C}} \text{Cos} \left(\frac{C_n}{\bar{C}} v \right) \right] \right\} \\ & - \frac{B_n C_n}{(1/a)^2 + (C_n/\bar{C})^2} \left[\frac{1}{a} \text{Cos} \left(\frac{C_n}{\bar{C}} v \right) - \frac{C_n}{\bar{C}} \text{Sin} \left(\frac{C_n}{\bar{C}} v \right) \right] \right\} \end{aligned} \right.$$

Since a plane wave is assumed, the stress may be obtained from Eqs. (4) and (15).

By using Eq. (15), the strain magnitude as a function of time at any location x may be obtained by allowing t to vary from $t = 0$ to $t = t_1$. It is meaningless to consider times for t greater than t_1 , since t_1 is defined as being the time required for the wave to completely propagate through the cone. The quotient given by the length of the cone (a) divided by the wave propagation speed (\bar{C}) defines t_1 for any given length of cone. Therefore, the applied strain at the base described by

the Fourier series will need Fourier coefficients A_0 , A_n , B_n , and C_n determined only for the period $t = 0$ to $t = t_1$.

A compression wave propagating from the base to the apex of a cone will develop a tensile tail so that momentum in the rod will be conserved (Ref. 7). Equation (15) predicts such a wave shape change.

Donnell (Ref. 6) has treated the wave propagation condition for the case of a gradual, arbitrary cross-sectional area variation. By considering that the gradual area change was brought about by n successive sudden changes and then letting n approach infinity, Donnell has shown that the strain transmitted forward at any station x is given by

$$\epsilon_x = \sqrt{\frac{A_{\text{base}}}{A_x}} \quad \epsilon_{\text{base}} = \frac{d_b}{d_x} \epsilon_{\text{base}} \quad (16)$$

No wave shape change is predicted by Eq. (16); therefore, it is only used herein to predict the maximum strain transmitted. For the conditions of the present tests, Eq. (16) predicts somewhat greater strain amplification than normalized results from Eq. (15).

2.2 WAVE PROPAGATION IN A BIMETALLIC CONICAL BAR WITH THREADED JOINTS

The preceding analysis is applicable to elastic stress wave propagation in a single-material, homogeneous, isotropic cone. However, many conical models are constructed of two or more materials. The schematic of a typical bimetal model is shown in Fig. 3b.

This model has two major discontinuities so far as one-dimensional stress wave propagation is concerned. The first discontinuity occurs at x_1 , and this discontinuity is the bottom of the hole for the nose tip screw. Because the end of the threaded section does not contact the bottom of the hole, the bottom of the hole acts as a free surface to part of the advancing stress wave. Thus, the portion of the incoming stress wave that impinges on the bottom of the hole is completely reflected. This essentially insulates the threaded section of the tip from the stress wave as it propagates toward the tip. Consequently, only the threaded portion of the base section between x_1 and x_2 is actively carrying the stress wave. That is, there is an abrupt area change effect at x_1 and a gradual area change effect from x_1 to x_2 . At x_2 , where the external portion of the tip begins, there is generally both an abrupt area change and a material difference.

The following analysis of stress wave transmission and reflection at a cross-section discontinuity has been used by various investigators (Refs. 6, 16, and 17). Consider the situation depicted schematically in Fig. 5. It has been shown that the stress magnitude of the incident wave, which is transmitted from A to B, is

$$\sigma_{\text{trans}} = \left(\frac{2r_{AB}}{r_{AB} + 1} \right) \frac{A_A}{A_B} \sigma \quad (17)$$

The strain transmitted from A to B is

$$\epsilon_{\text{trans}} = \left(\frac{2r_{AB}}{r_{AB} + 1} \right) \frac{A_A}{A_B} \frac{E_A}{E_B} \epsilon \quad (18)$$

Also, the stress and strain reflected at the discontinuity are, respectively,

$$\sigma_{\text{refl}} = \left(\frac{r_{AB} - 1}{r_{AB} + 1} \right) \sigma \quad (19)$$

$$\epsilon_{\text{refl}} = \left(\frac{r_{AB} - 1}{r_{AB} + 1} \right) \epsilon \quad (20)$$

where

$$r_{AB} = \frac{A_B \rho_B \bar{C}_B}{A_A \rho_A \bar{C}_A}$$

A = cross-sectional area

ρ = mass density

\bar{C} = E/ρ = stress wave propagation velocity in a slender rod

Equation (18) may be used to compute the transmitted strain ($\epsilon_{1\text{trans}}$) at point x_1 .

The analysis of Section 2.1 may be applied to the model base section between $x = 0$ and $x = x_1$. However, this analysis does not apply to the model section from x_1 to x_2 . In this midsection, the effective cross-sectional area is given by

$$A_{x_{\text{eff}}} = A_x - A_t \quad (22)$$

where

$$A_x = (\pi/4)d_x^2 = \text{cross-sectional area of cone at } x$$

$$A_t = (\pi/4)d_t^2 = \text{cross-sectional area of thread}$$

Donnell's analysis (Ref. 6) may be applied to the threaded section between x_1 and x_2 . In this case, Donnell's result for the strain transmitted forward at any station x is

$$\epsilon_x = \sqrt{\frac{A_{x_1} - A_t}{A_x - A_t}} \epsilon_{1\text{trans}} \quad (23)$$

where

$$\epsilon_{1\text{trans}} = \text{strain transmitted across discontinuity at station } x_1$$

$$A_{x_1} = \text{cross-sectional area of cone at } x_1$$

No change in wave shape is predicted by Eq. (23); therefore, it is only used herein to compute the maximum strains transmitted forward in the threaded region.

The above analysis predicts the same level of maximum strain in the threaded section (x_1 to x_2) regardless of the tip material, because strain reflection from the x_2 junction has not been taken into account. This discontinuity will reflect a portion of the incoming compression strain back into the threaded section as a compression strain. This reflected strain will combine with the incoming strain to intensify the compression strain level. The apparent wave shape as sensed by the gages will be a distorted one.

Because the gages in the threaded section are no more than 0.32 in. from x_2 , it requires no more than 1.6 μsec , or less, for the reflected wave to reach the gages. The duration of the maximum strain level of the pulse is at least 3.5 μsec or more (Figures 11 through 16). This is ample time for a portion of the maximum strain to be reflected at x_2 and reach the gages in the threaded section while the incoming strain is still maximum or near maximum at those points. The following analysis is made under the assumption that the maximum compressive strain has been intensified by reflection of a portion of the maximum compressive strain. However, in general, it must be noted that the

amount of strain amplification caused by reflection is highly dependent on the shape of the wave.

Equation (20) may be used to calculate the reflected strain at $x_2(\epsilon_{2_refl})$. Donnell's theory applied to the amplification (or decrease) of the reflected strain in the threaded section yields

$$\epsilon_{x_refl} = \sqrt{\frac{A_{x_2} - A_t}{A_x - A_t}} \epsilon_{2_refl} \quad (24)$$

The sum of the results from Eqs. (23) and (24) for the threaded section predicts the total maximum compressive strain experienced by this important part of the specimen.

The analysis of Section 2.1 applies to the conical tip section of the model from x_2 to the apex. The base input strain required is the strain transmitted across the discontinuity at x_2 , which may be computed by Eq. (18).

Table I (Appendix II) lists the material properties of the specimens. Tables II and III list the strain transmission and reflectivity parameters for the discontinuities at x_1 and x_2 , respectively, for all the specimens. Table IV contains the cross-sectional area characteristics for each specimen which are necessary for application of Donnell's analysis. Tables V through VIII contain final results of the Donnell and the combined Fourier-Donnell prediction of the compressive strain amplification factors for each test specimen.

The foregoing comments concerning stress wave transmission and reflection from Station x_2 to the tip apply only to the case of a 90-deg tip attachment angle (Fig. 3b). When a stress wave impacts a boundary (material change or free surface) at other than a normal incidence angle, various other equations must be considered (Ref. 7). It has been shown that when an elastic stress wave hits an interface at other than normal incidence, then four stress waves are generated. Two of these stress waves are transmitted into the second medium and two are reflected back into the first medium. Even with radial symmetry existing, the wave propagation geometry is two-dimensional, and the analysis is rather complex. Consequently, no quantitative theoretical predictions are made for the stress wave behavior of the model tip section with the 45-deg attachment angle. Some intuitive observations will be made in Section IV.

SECTION III EXPERIMENTAL PROGRAM

3.1 SCOPE OF INVESTIGATION

The initial experimental test program had four main objectives. The first objective was to determine the effect that cone angle has on strain wave propagation from the base to the apex of a solid cone with no joints. Cone semi-angles of 2, 5, 7.5, and 10 deg were utilized. These conical test specimens were constructed of 7075-T6 aluminum alloy.

The second objective was to determine the effect of a typical threaded joint on the strain wave propagation in a cone. For these tests, the 7075-T6 aluminum alloy cone had a tip of the same material. These test specimens had cone semi-angles of 2 and 10 deg. The effect of tip attachment angle was investigated by testing tips with 0- and 45-deg attachment angles.

The third objective was to ascertain the effect of a cone tip constructed from a different metal than the base of the cone (i. e., a so-called bimetal cone). Jointed models were tested with beryllium-copper and Fansteel 60[®] tips. The cone base in all cases was 7075-T6 aluminum alloy. These models had cone semi-angles of 2 and 10 deg. Tip attachment angles of 0 and 45 deg were also used in bimetal specimen construction.

The fourth objective was to ascertain the applicability and limitations of the one-dimensional theory described in Section II. In other words, can this relatively simple theory be used in conical model design, and if so, what are its limitations? These questions are answered by comparing the theoretical predictions with the data from the experimental program.

3.2 TEST APPARATUS

Typical test bars used to determine the effects of cone angle on longitudinal wave propagation from the base toward the cone tip are shown in Fig. 6. The test bars were basically Hopkinson pressure bars (Ref. 3) with a cone machined on one end. All of the test bars used for this phase of the investigation were machined from a 7075-T6

aluminum alloy bar that possessed a tensile yield strength of 74,000 psi, a tensile ultimate strength of 81,800 psi, and a tensile modulus of elasticity of 10,400,000 psi.

Strain magnitudes were measured using foil electric resistance strain gages placed on the surface of the test bars. The gages had a gage length of 0.131 inches, a resistance of 120.0 ohms, and a gage factor (G) of 1.96. The gages were bonded to the bar surface using a room temperature curing epoxy cement.

Gages were placed on the cone and cylindrical section surfaces of the solid test bars to measure strains in the longitudinal direction and at 90 deg to the longitudinal direction for the 5-, 7.5-, and 10-deg test cones. Only longitudinal strains were measured on the 2-deg test cone. The location of the gages on a typical test bar is shown in Fig. 6. The longitudinal gage locations have been numbered in numerical order starting with the gage nearest the impact surface (flat end of cylindrical section) as number one. Since lateral strains were measured at only two locations, the gage on the cylinder is referred to as gage number 1.2, and the gage on the cone surface is referred to as gage number 1.3.

Two gages were placed at each location for measuring longitudinal strains. They were placed on opposite sides of the bar, or 180 deg apart, so that when connected into the Wheatstone bridge circuit, bending effects in the test bars would be nulled. Only one gage was used for measuring lateral strains at each of the two points.

The test bars used to determine the effects of a typical thread joint and bimetal cone construction are shown in Fig. 7. The cylindrical and conical base sections were machined from a 7075-T6 aluminum bar. The materials used for the nose tips were 7075-T6 aluminum, beryllium-copper, and a tantalum-tungsten alloy (Fansteel 60). Pertinent properties of these materials are listed in Table I.

The jointed cones were instrumented with two or three strain rosettes and two or more longitudinal strain gages, as shown in Fig. 7 for both the 2- and the 10-deg semi-angle test bars. The rosettes consisted of three gages placed in a standard 45-deg orientation. All were 1/32-in. gages except for the 1/8-in. longitudinal and transverse gages of rosettes (1R) and (3R) on the 2-deg semi-angle cone specimen.

The cylindrical section of each bar acted as a wave guide which transmitted the wave to the cone base. The length of the cylindrical section was six times the bar diameter, or greater, for all bars to allow the impulse some opportunity for smoothing (by internal material damping) before contacting the conical base. Also, the cylinder allowed the wave to be monitored prior to its arrival at the cone base, which will be discussed in more detail later.

A pulse was imparted to the flat end of the cylindrical section of the test bar by the impact of a flat end solid projectile 1.0 in. long and 1.31 in. in diameter. The projectile was made of the same material as the test bars.

An air-operated gun was used for launching the projectile and supporting the test bar during the impact cycle. Figure 8 shows a sectional view of the gun with the projectile and test bar installed in position for a typical operation. The velocity of the projectile was maintained at a low level such that the maximum observed stress on the cylinder never exceeded 10,000 psi. Since the applied force was not great enough to cause plastic deformation in either the projectile or test bar impact surfaces, the only special consideration given to the surfaces was to ensure that they were machined flat and perpendicular to their longitudinal axis to within 0.001-in. total indicator reading.

The Wheatstone bridge circuits and means of amplifying and recording the signal from the strain gages used to measure longitudinal strains are schematically shown in Fig. 9. The circuit and recording procedures for the individual gages in the rosettes were similar except one gage was replaced with a 120-ohm resistor.

The electrical circuit was designed to eliminate electrical noise in the bridge by sensing voltages e_A and e_B , and then feeding them into a high gain differential amplifier which subtracted out voltages common to each leg of the bridge. The voltage e_{out} , fed out of the differential amplifier to the oscilloscope represents the difference between e_A and e_B and is the voltage across the bridge resulting from strain-gage excitations.

The signal from the amplifier was fed to a dual-beam oscilloscope and displayed on a cathode-ray tube (CRT). The output beam signal trace was photographed using a Polaroid camera attached to the scope face.

3.3 EXPERIMENTAL PROCEDURE

During each test, the following sequence of events was performed. First, the air gun was put in a prefire condition by replacing the diaphragm and positioning the projectile in the launch tube against the diaphragm holder. The test bar was then slipped into the opening provided at the end of the launch tube until it was one-fourth of one inch from the muzzle of the launch tube. The small rectangular transverse opening through the launch tube wall enabled one to determine the location of the test bar before each test.

After restoring the gun to prefire conditions, the strain gages were connected into their individual bridge circuits as shown in Fig. 9. The bridges were then balanced by adjusting the 0- to 50-ohm potentiometer provided in each circuit until a zero voltage was indicated on the oscilloscope CRT. When the bridges were all balanced, the voltage output from the strain gages displayed on the CRT was calibrated to represent strain directly using standard techniques. After calibrating the strain-gage output, the oscilloscopes were set to sweep at a rate that permitted recording the initial forward propagation of the wave and its reflection.

In order to measure strains at the various locations along the bar as the wave front made its initial pass, the oscilloscopes were triggered to begin their sweep just prior to the arrival of the wave at the cone base. The output of the first strain gage on the cylindrical section of the bar that the wave encountered was utilized as the trigger voltage for all oscilloscopes to simultaneously begin their sweep. No delayed sweeps were necessary because of the relatively short transit time between gages. Since the output voltage was a result of the unbalance in the Wheatstone bridge circuit caused by the wave, it meant that the leading edge of the wave at the first gage would be chopped off since the sweep would not have started until the level of voltage required to trigger the sweep circuits was reached. Consequently, the output voltage required to trigger the sweep circuits was set as low as the circuit would permit in order to obtain as much information as possible about the strain magnitude at the first gage. Therefore, the first gages to measure the full wave were the second set of gages located on the cylindrical section of the test bar. This made it possible to obtain at each gage point a complete time behavior of the strain as it passed.

After ensuring that the data recording equipment was properly set, the gun driver gas chamber was charged to 14 psig. The charge line valves were then closed. Immediately after closing the charge line

valves, the solenoid valve used to open the air lines for actuating the diaphragm breaker was opened. The diaphragm breaker punctured the diaphragm, allowing the driver gas to expand by accelerating the projectile until impact between the projectile and test bar occurred. The photographs of the oscilloscope traces were then collected, and all necessary information was recorded.

An effort was made to impart a plane wave to the cones by maintaining alignment of the projectile with the test bar when impact occurred. Since it is difficult to generate an absolutely plane impact between the projectile and the test bar each time, it was decided to determine by experiment approximately how much the direction of the principal strains varied from the axis of symmetry of the test bars. This was done by comparing strains obtained from two different sets of gages placed on a cylinder that was one inch in diameter, twelve inches long, and made of the same material as the test bars (Fig. 10). One set of gages was placed on the cylinder to measure longitudinal and normal strains in identically the same way as was done on the test specimen. When gages are placed this way, it is assumed that the principal strains occur along the axis of symmetry of the cylinder. The second set of gages was a three-element rosette made up of strain gages with the same gage length and gage electrical characteristics as was the first set. The three-element rosette enables one to calculate the principal strains and their direction. The location of the gages and their orientation are shown in Fig. 10.

The directions of the principal strains determined from the three-element rosette data indicated that the deviation of the direction of the principal strains from the directions of symmetry for the test bars ranged from two minutes to one degree. However, the variation in the magnitude of the principal strains with that obtained from the gages used for obtaining data for this research was negligible. Consequently, essentially a plane wave was applied at the base of each cone, unless explicitly stated otherwise.

3.4 DATA REDUCTION PROCEDURE

A Benson-Lehner film reading machine was used to read all of the strain data from the Polaroid film. This particular film reader uses a parallel beam of light to backlight the oscilloscope traces. The image of the CRT traces and grid is in turn projected onto a light diffusion board where vertical and horizontal crosshairs were positioned to define

points on the trace. Since the film reader had the capability of giving x and y locations of points, it was necessary to select a reference point for referencing all data. Generally, the reference point was taken at the extreme left of each trace where time (t) = 0.

The accuracy and repeatability of the film reading machine are influenced by the operator to some extent. To determine the operator influence on data repeatability, two sets of readings were obtained for the 2- and 7.5-deg cone data by two different, experienced operators. The readings all fell within a range of ± 0.5 percent of the mean reading. Therefore, it is believed that the error introduced by the film reader operator was within ± 0.5 percent.

Data obtained from gages used for measuring strain in the longitudinal and lateral directions were taken at face value and used as received. For strain-gage rosettes, the data read from the photograph were input to a 45-deg rosette data reduction program which calculated the principal stresses, the direction of the principal stresses, and the maximum shear stresses. Generally, the strain magnitude was greatest when the wave made its initial pass through the cone. Consequently, only that part of the trace was analyzed in detail.

3.5 ERROR ANALYSIS

An error analysis of the experimental apparatus and data reduction procedure was presented in Ref. 4. The results of this analysis are given below:

Experimental Error Summary

Calibration Resistor	1.0%
Oscilloscope Calibration	5.0%
Strain Distortion Caused by Dynamic Environment (Ref. 18, pp. 225-227)	<1.0%
Film Reader Operator	<u>0.5%</u>
Total	<7.5%

The total error shown is conservative in that it is based on every contributing factor being at either its plus or minus maximum deviation simultaneously. This combination would seldom occur in practice, so it is believed that the total precision error is less than 5 percent.

SECTION IV DISCUSSION OF RESULTS

4.1 SOLID CONES

Typical examples of the experimental data obtained from the 2-, 5-, 7.5- and 10-deg semi-angle solid cones are presented in Figs. 11 through 16. These figures show strain variation with time at the various observation points on the test bars as the wave made its initial pass through the cone from the base to the apex. Zero time in these figures corresponds to the wave leading edge arrival time at the base of the cone. The time between strains at the various gage points represents the propagation time between points. The wave propagation velocity (\bar{C}) was observed to be 0.193 in./ μ sec (16,100 ft/sec) which agrees very closely with the theoretical value of 0.198 in./ μ sec (16,600 ft/sec) from Eq. 2.

The applied wave shape and magnitude (shown in Fig. 11, for example) was actually observed at Gage Number 2 on the cylindrical section of the test specimen. In all cases, the peak magnitude is greater than that observed at Gage Number 3 which was on the cone surface near the base. The probable explanation for this apparent strain reduction is that, when the wave arrives at the cone-cylinder intersection, a portion of the wave is reflected because of the change in cross section. This creates a reduction in the strain magnitude which actually enters the cone.

The 2-deg semi-angle cone data for a wave propagating from the base to the apex exhibits a behavior similar to a spherical converging wave (Refs. 5, 7, and 12). As the wave traveled from the base toward the apex, the initially fully compressive shape was transformed into one with a leading compressive component and a trailing tensile component. The compressive component is shortened in width and increased in height as the apex is approached. The magnitude of the trailing tensile strain component increased as the apex was approached and was observed to exceed the compressive strains near the cone apex. The one-dimensional theory also predicts these characteristics as shown in Fig. 12. After it reaches the apex, the pulse then travels back toward the base as a tensile wave (with a trailing compressive portion). If these tensile stresses exceed the elastic limit of the material, total deformation or even tip separation may occur. These same phenomena have also been observed experimentally by Kolsky (Ref. 7), Goldsmith (Ref. 12), and Sharpe (Ref. 15).

Stress-strain pulses with long wave lengths in large semi-angle cones (≈ 10 deg) exhibit reflection characteristics similar to those of flat-ended cylindrical rods. It is well known, both theoretically and experimentally, that plane dilatational waves traveling in cylindrical rods will be reflected at the flat end with a change in phase only (sign reversal). Except for perhaps small effects of internal solid damping, the absolute value of the reflected wave will be unchanged. This type of reflection pattern was observed in the 10-deg semi-angle cone. However, the magnitude of the tensile and compressive components decreased as the apex was approached, which indicated that the sloping lateral surface of the cone was causing a noticeable portion of the wave to be reflected at each point. Consequently, the absolute value of the strain (both compressive and tensile) did not greatly exceed, or were actually less) than the input to the base. This feature of the large angle cones is dependent on the pulse length, but it does enable the large angle cones to sustain greater transient loads than the sharper cones. This is fortunate and of practical importance in model design. The two intermediate cone specimen (5- and 7.5-deg semi-angle) exhibited propagation characteristics somewhat between the 2- and the 10-deg specimens.

Three of the test specimens (5, 7.5, and 10 deg) had gages placed 90 deg to the longitudinal gages at positions 2 and 3 (Fig. 6). The strains measured by these gages were ratioed with the longitudinal strains measured at these same locations. These ratios varied from 0.28 to 0.33, which is basically the range of values found in the literature for Poisson's ratio. These results tend to confirm the basic theoretical assumption that the wave was essentially one dimensional at least during its first trip from the base to the apex.

Figures 17 to 20 contain a comparison of the experimental data with results from one-dimensional theory (Section 2.1). This comparison is based on normalized values defined as compressive strain amplification factors. Mathematically this is stated as follows:

$$\text{C.A.F.} = \epsilon_x / \epsilon_{\text{base}} \quad (25)$$

where ϵ_x is the maximum compressive strain observed at a particular location and ϵ_{base} is the maximum compressive strain applied at the cone base. In reality ϵ_{base} was observed at gage number 2 on the cylindrical portion of the test specimen unless noted otherwise.

Two different theoretical predictions are shown on each figure. These are: (1) Donnell's Analysis (Eq. (16)), and (2) Fourier Analysis (Eq. (15)). The Donnell theory predicts greater strain amplification than the Fourier analysis. The difference is large near the cone tip, even for the 5-deg semi-angle cone. The discrepancy becomes larger as the cone angle is increased. The Donnell analysis does not take the wave shape change into account, and this is believed to be a primary reason for the discrepancy in the two theoretical results. Wave shape (and/or duration) affects strain amplification more for the large angle cones than it does for slender cones.

The Fourier theory predicts both the trend and magnitude of the compressive stress amplification for the 2-deg half-angle cone very well indeed (Fig. 17). The Fourier theory also predicts the trend of the strain amplification for 5-, 7.5-, and 10-deg half-angle cones. However, the predicted magnitude is somewhat larger than the experimental data indicate.

It is believed that a portion of this discrepancy in magnitude is created by using the output from gage 2 on the cylinder as the input forcing function to the theoretical calculation (Eq. (8)). Actually a gage should have been placed on the conical surface immediately adjacent to the cylinder-cone junction. The output from this gage would then be used to represent the forcing function and to normalize the experimental data. There is a reflection at this junction so that the complete wave amplitude in the cylindrical section did not enter the cone. Consequently, this makes the predicted values high and the experimental normalized data low by comparison. This effect is particularly noticeable for the large angle cones (Figs. 18, 19, and 20). Later tests were conducted with a 10-deg half-angle jointed cone which had a gage just forward of the cone cylinder junction (gage 1, Fig. 7). These data, when normalized by the gage 1 output, gave amplification factors higher than predicted by theory (see Section 4.2, experimental data, for 10-deg half-angle cones, just forward of gage 1). From the above arguments then, it is believed that the theory predicts both the trend and magnitude of the compressive strain amplification very well for the small angle cone and reasonably well for the large angle cone.

No results are presented for the tensile strain amplification factors, but the data trends and amplitudes are very similar to those shown for the compressive strains.

4.2 JOINTED CONES

Experimental and theoretical results for compressive stress amplification factors are shown in Figs. 21 to 25 for the cones with tip joints. The tip attachment angle was 90 deg (Fig. 3) for these specimens. Two different theoretical predictions are shown in each figure:

1. Donnell's Analysis applied to both the solid cross sections and the threaded section (Tables V and VI).
2. Combined Fourier-Donnell Analysis. The present Fourier solution is applied to the solid cross sections (base and tip) and Donnell's theory is applied to the threaded section (Tables VII and VIII).

The appropriate strain transmission and reflection factors at a discontinuity are included in the theoretical predictions.

The effect of a threaded juncture alone without different tip materials is shown in Fig. 21 for the 2-deg half-angle cone. Although it may be somewhat fortuitous, the agreement between theory and experiment for this specimen is considered very good, particularly the transmitted strain to the tip from x_2 compared with the combined Fourier-Donnell Analysis. It is believed that a very good joint contact at x_2 existed for this model. The reflected strain at x_2 also depends on the joint contact. Theory predicts that about 28 percent of the strain at x_2 is reflected back into the threaded section. The experimental results substantiate this amount of strain reflection.

The effect of heavy metal tips is to intensify the strain in the threaded section because of increased strain reflection at x_2 (Figs. 22 and 23). The theoretical prediction of the total amplification in the threaded section is quite good for the beryllium-copper tip (Fig. 22) but is about 30 percent low for Fansteel 60 tip (Fig. 23). In contrast, the strain transmitted across x_2 to the tip for the beryllium-copper model is somewhat higher than predicted, while the transmitted strain for the Fansteel 60 tip agrees reasonably well with theory.

It was noted in Section 4.1 that increasing the cone half-angle reduces the strain amplification for solid cones. This trend is also quite evident for the 10-deg semi-angle jointed cones (Figs. 24 and 25) when compared with the 2-deg semi-angle cones (Figs. 22 and 23). The combined Fourier-Donnell Analysis (with reflection at x_2) agrees reasonably

well with the experimental results from the beryllium-copper specimen (Fig. 24). This also applies to the Fansteel 60 model (Fig. 25) except for the experimental data from gage 5 (forward gage) in the threaded section. The strain at this point is double that predicted by the combined Fourier-Donnell Analysis and nearly 50 percent more than predicted by Donnell's analysis. This is somewhat consistent with results for the Fansteel 60 tip on the 2-deg cone (Fig. 23). Perhaps these discrepancies between present theory and experiment could be explained by a more refined analysis which took wave shape effects in the threaded section into account.

The Donnell Analysis yields somewhat higher (and hence more conservative) strain amplification factors than the Combined Fourier-Donnell Analysis. The Donnell Analysis is not restricted to cones and is relatively simple to apply since only the model cross-sectional dimensions are required. As such, it should lend itself well to preliminary model design investigations for jointed cones. It is obvious that strain reflection at x_2 type joints makes an important contribution to the compressive strain amplification in the threaded region. Thus, a theoretical investigation which takes wave shape effects in the threaded section into account is highly justifiable. Additional experimental work on stress-strain propagation in various other types of joints (i. e., bonded or glued) would also be quite valuable for model design purposes. In particular, various types of joint buffers should be investigated to see if the reflected and transmitted strains can be dissipated somewhat.

Tensile strain amplification factors for the jointed models are not presented, but the amplitudes are similar to those presented for compressive strains. Also experimental data were acquired for specimens where the tip attachment angle was 45 deg. The general level and the scatter of these data are essentially the same as that for the zero attachment angle. Consequently, no discernible difference existed between data for the two attachment angles.

There are practical considerations which have led to the abandonment of the 45-deg tip design, however. As the compressive wave reaches the outer lip of the joint, Poisson's effect creates a radial tensile strain in the material. This tensile strain tends to spread the tips of the joint as illustrated in Fig. 26. Since the base portion cross-sectional area approaches zero at the joint lip, stress can be very high and permanent deformation may result. There were no strain gages placed on the joint lip of the present models. If gages had been placed there, no doubt they would have been subjected to rather large plastic

strain. For the 90-deg tip attachment angle, no very small areas exist at the joint, and permanent deformation is less likely.

The experimental results discussed up to this point have all been for plane wave propagation in the test bar (see Section 3.3). A so-called "nearly perfect" plane wave is very difficult, if not impossible, to generate even under controlled laboratory conditions. As such, it is believed that non-planar stress-strain waves in the model occur during the actual light gas gun launch cycle. This can easily occur because of imperfect fits of sabot and/or model joints. For this reason, the unsymmetrical load application is of practical importance. During planar wave propagation, the initial compressive wave and tensile tail always have the highest peak values of strain with each successive reflection attenuated somewhat. In the case of non-planar waves, the highest peak amplitude normally occurs on one of the successive reflections. That is, the greatest stress (or strain) magnitude occurs during one of the reflections as the wave travels back and forth along the model length. Thus, model failure caused by unsymmetrical stresses may occur in a random fashion.

These non-planar waves with their very high strain amplifications frequently caused plastic deformations in the test specimen tips during the experiments. These plastic deformations were large enough to be observed without any visual magnification. Plastic deformation of conical model tips has been observed during ballistic range testing (Fig. 2). Thus it is evident that during design and manufacture of actual models, reasonable effort should be made to ensure that the stress wave will propagate symmetrically in the model. (Model-sabot contact areas and model joints are critical items.) Consequently, it is strongly recommended that experimental and theoretical investigations be conducted to ascertain the effect of sabot geometry on stress-strain propagation in the projectile.

SECTION V CONCLUSIONS

An experimental and theoretical investigation of strain propagation in solid and jointed conical rods which simulate actual gun-launched models has been conducted. As a result of this investigation, the following conclusions are drawn:

1. Increasing the cone semi-angle from 2 to 10 deg reduces the general level of strain (or stress) amplification in the tip region, that is, the larger the cone angle, the less likely it is to fail under launch conditions. This applies to both solid and jointed cones.
2. The effect of a threaded joint is to increase the strain (or stress) in the outer threaded section of the base because of (a) an area reduction and (b) reflected strain from the tip junction back into the threaded section.
3. Tips made of heavier, denser metal than the base greatly intensify the strain in the outer threaded base section. This is because a large percentage of the high level compressive stress is reflected back upon itself and thus the total strain level is almost doubled. It must be emphasized that the amount of amplification from reflection is highly dependent on the strain pulse shape and duration.
4. A solution (Eq. (15)) to the one-dimensional wave equation for strain propagation in cones (Eq. (1)) was developed, based on a rather general Fourier series representation of the transient strain input to the cone base (herein called the Fourier solution). This solution agreed very well with the experimental results for the 2-deg cones. When applied to the larger angle solid cones, the general trend of strain amplitude was predicted quite well, but the strain magnitude prediction can only be considered fair.
5. Donnell's solution for strain transmission in cones (Eq. (16)) generally gave a somewhat larger strain amplification factor than the Fourier solution, the difference being greater for the large cone angles. Donnell's theory could also be applied to the threaded section (Eqs. (23) and (24)). When used for both solid and threaded sections of the jointed cones, Donnell's theory predicted strain amplification factors that were somewhat higher than predicted by a hybrid analysis called the combined Fourier-Donnell method. This consisted of the Fourier solution for the solid section combined with Donnell's results for the threaded section.

6. The general level of experimental strain amplification for the important threaded region (x_1 to x_2) of the jointed cones (7075-T6 and Be-Cu) was estimated reasonably well by either one or both of the analysis methods (Donnell or combined Fourier-Donnell with strain reflection at x_2 considered). The exception to this was the models with Fansteel 60 tips. A more refined analysis (considering wave shape effects and/or additional reflections) is required to account for the rather large discrepancy between present theory and experiment in the threaded section for Fansteel 60 tip joints. Judicious application of the Donnell theory should suffice for most model preliminary design analysis. It has the advantage of being simple and easy to apply, requiring only the model geometric characteristics.
7. Joints with angles of 45 deg are not recommended for use in model design, since excessive distortion takes place at the important and critical joint lip area. This distortion was visible to the unaided eye and would certainly affect flight performance.
8. Non-planar strain pulses caused higher strain amplification factors in the models than planar pulses. The peak amplification from the non-planar waves occurred on one of the reflections as the wave traveled back and forth along the length of the cone, whereas the plane waves had the highest amplification during the initial forward travel. The non-planar waves with their very high strain magnification frequency caused visible plastic deformation (bending) in the model tips. Reasonable effort should be made to ensure symmetrical stress-strain propagation in actual models.

REFERENCES

1. Cable, A. J. and DeWitt, J. R. "Optimizing and Scaling of Hypervelocity Launchers and Comparison with Measured Data." AEDC-TR-67-82 (AD812849), April 1967.
2. Cable, A. J. "An Examination of Failing Loads in Model Launching Experiments." AEDC-TR-65-54 (AD457907), April 1965.

3. Evans, P. A. "An Investigation of Elastic Strain Wave Propagation in Conical Bodies." M.S. Thesis in Mechanical Engineering, University of Tennessee Space Institute, March 1969.
4. Nenninger, R. L. "Stress Wave Propagation in Small Angle Bi-Metal Cones." M.S. Thesis in Aerospace Engineering, University of Tennessee Space Institute, December 1968.
5. Landon, J. W. and Quinney, H. "Experiments with the Hopkinson Pressure Bar." Proceedings of the Royal Society, A, Vol. 103, March 1923, pp. 622-643.
6. Donnell, L. H. "Longitudinal Wave Transmission and Impact." Transactions of the American Society of Mechanical Engineers, Vol. 52, 1930, pp. 153-167.
7. Kolsky, H. Stress Waves in Solids. Dover Publications, Inc., 1963, (First printed in 1953 by Clarendon Press, Oxford, England).
8. Vodicka, Vaclav. "Longitudinal Vibrations of a Conical Bar." Applied Scientific Research, Section A, Vol. 11, 1963, pp. 13-16.
9. Sur, S. P. "Longitudinal Propagation of Elastic Disturbance in a Conical Rod with Varying Elasticity." Rev. Roum. Sci. Techn. Mec. Appl., Tome 10, No. 3, Burcharest, 1965, pp. 593-599.
10. Wlodarczyk, E. "Propagation of Elastic-Plastic and Shock Waves in a Bar of Finite Length and Monotone Decreasing Cross-Sectional Area." Proceedings of Vibration Problems, Polish Academy of Sciences.
11. Brillhart, L. V. and Dally, J. W. "A Dynamic Photoelastic Investigation of Stress Wave Propagation in Cones." Experimental Mechanics, April 1968, pp. 145-153.
12. Kenner, V. H. and Goldsmith, W. "Elastic Waves in Truncated Cones." Experimental Mechanics, October 1968, pp. 442-449.
13. Lewis, J. L., Goldsmith, W., and Cunningham, D. M. "Internal-Strain Measurements of Longitudinal Pulses in Conical Bars." Experimental Mechanics, July 1969, pp. 313-320.
14. Yang, J.C.S. and Hassett, R. J. "Transient Stresses in Axisymmetric Bodies of Varying Area." Experimental Mechanics, July 1972, pp. 304-310.

15. Sharpe, W. N., Jr. "Fracture of Lucite Cones by Shock Waves." ASME Journal of Applied Mechanics, June 1972, pp. 390-394.
16. Rayleigh, Lord. Theory of Sound Vol. 1, Chapter 7, Dover Publications, 1945 (first published in 1877).
17. Ripperger, E. A. and Abramson, H. N. "Reflection and Transmission of Elastic Pulses in a Bar at a Discontinuity in Cross Section." Proceedings of the Third Midwestern Conference on Solid Mechanics, University of Michigan Press, 1957, pp. 135-145.
18. Dove, R. C. and Adams, Paul M. Experimental Stress Analysis and Motion Measurement, Charles E. Merrill Books, Inc., Columbus, Ohio, 1964, pp. 226-227.

APPENDIXES
I. ILLUSTRATIONS
II. TABLES

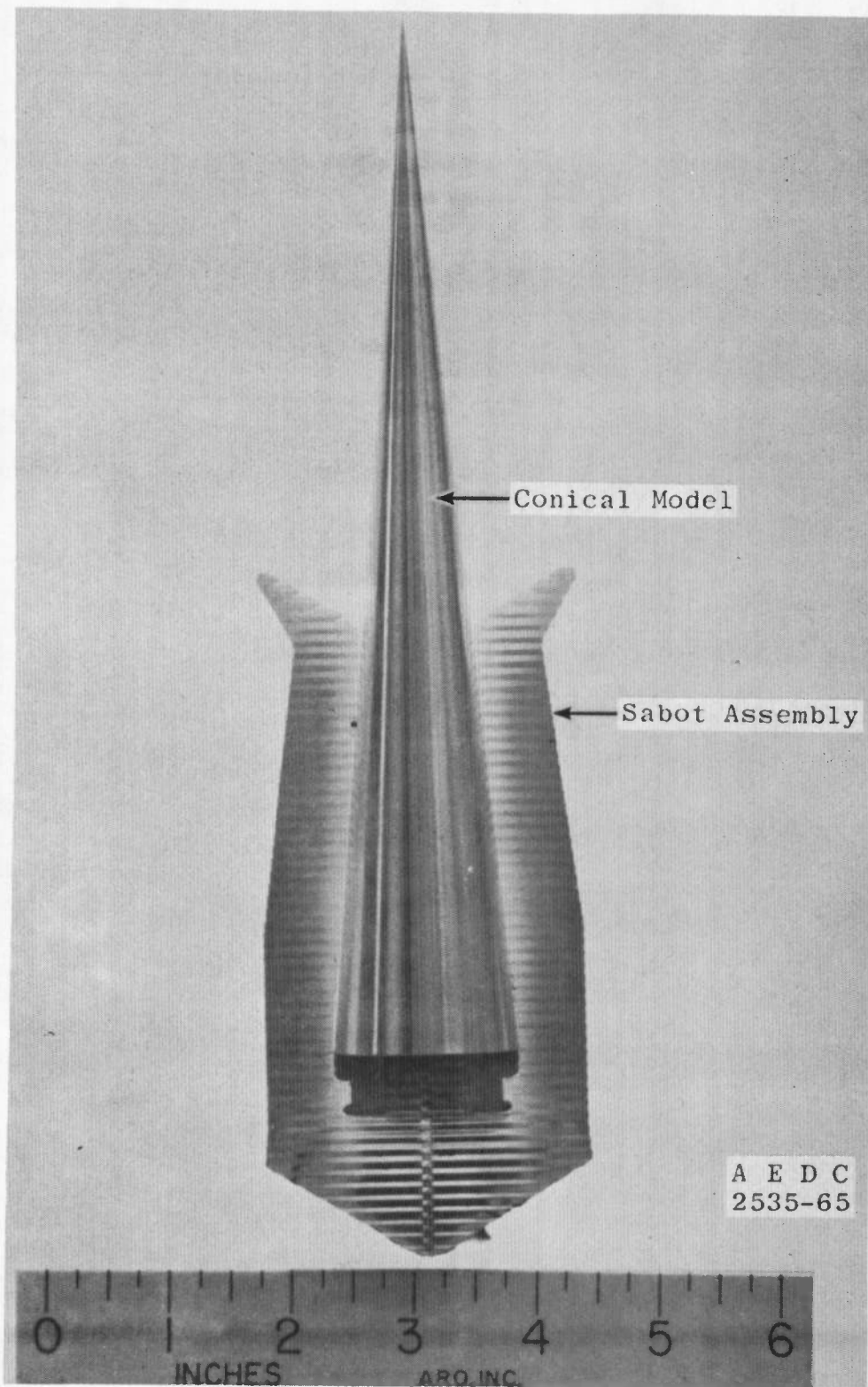


Fig. 1 A Typical 5-deg Semi-Angle Cone Model and Sabot

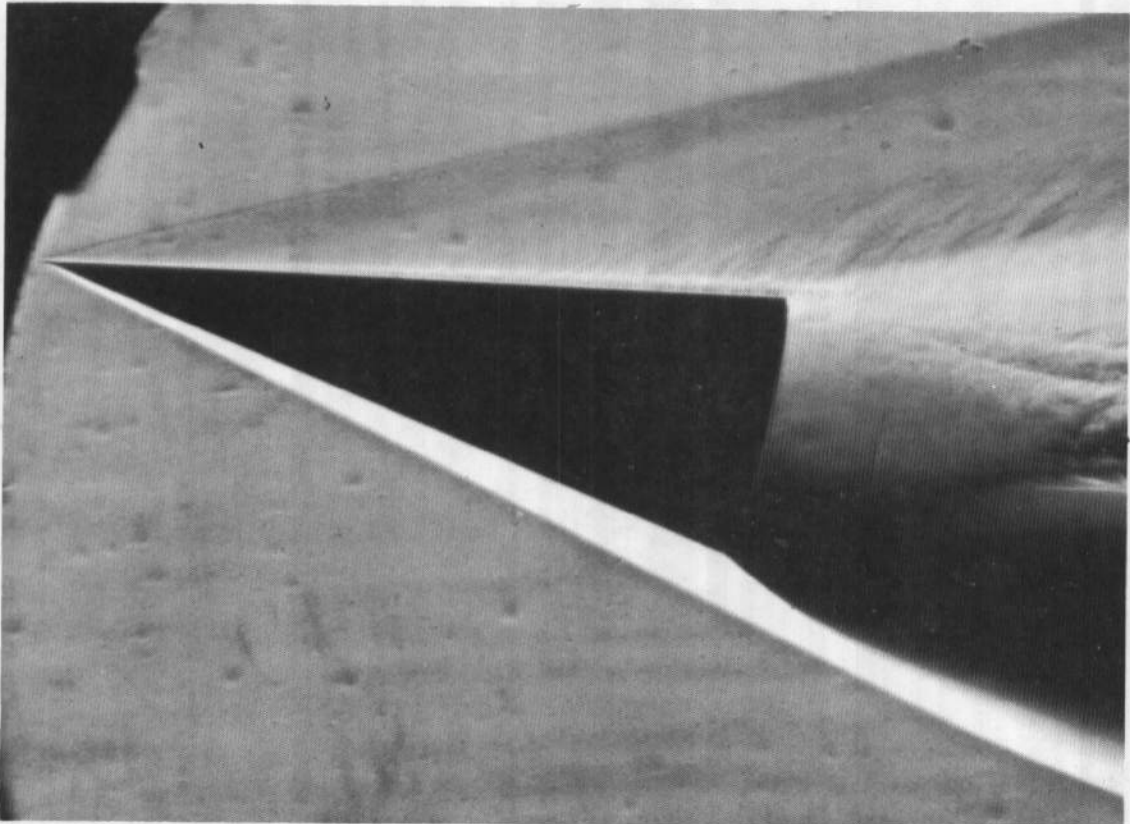
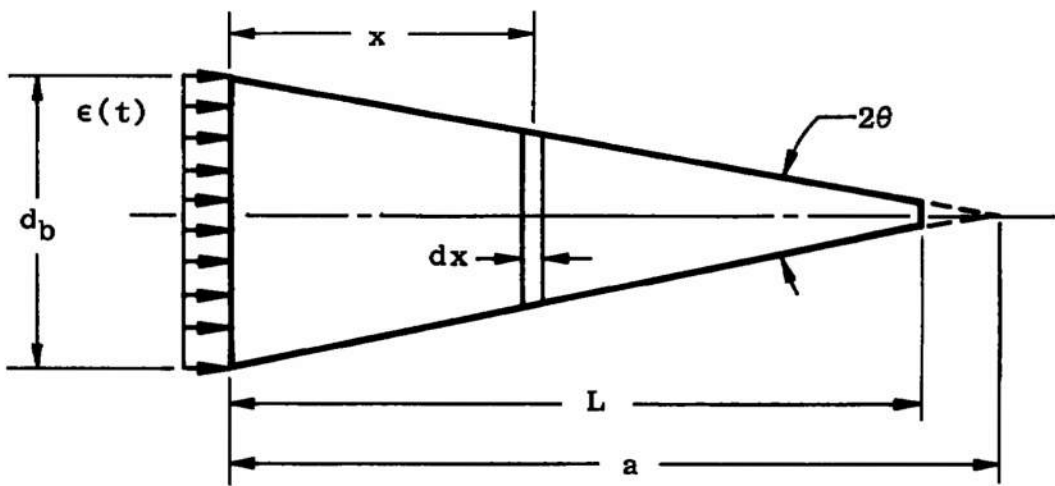
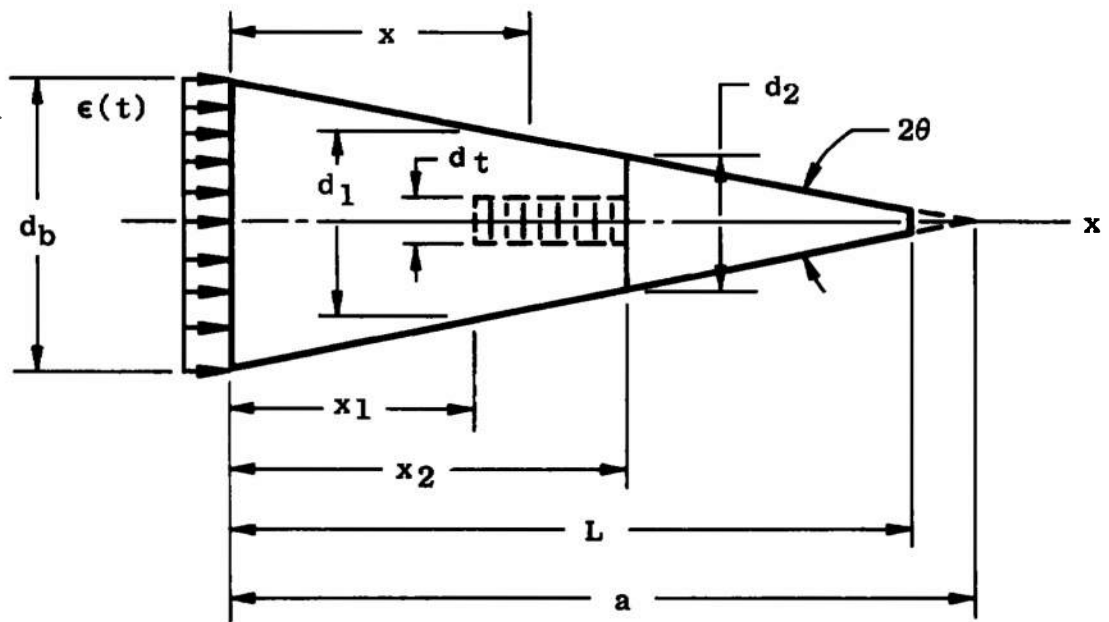


Fig. 2 Gun-Launched Model with Bent Nose Tip



a. Solid Cone Geometry



b. Jointed Cone Geometry (Tip Attachment Angle is 90 deg to X-Axis)
 Fig. 3 Sketch of Analytical Models

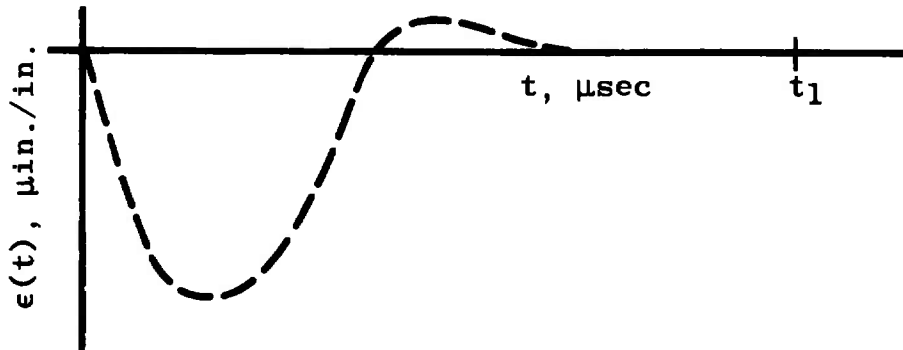


Fig. 4 Schematic Representation of Strain Impulse Applied to Base of Cone

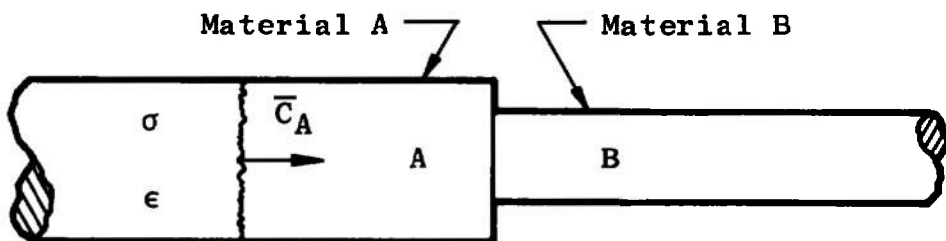
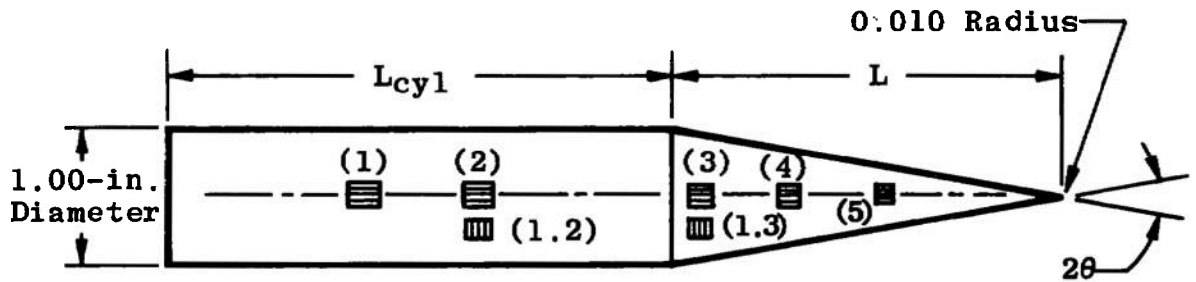


Fig. 5 Discontinuity Schematic



Notes: (1), (2), (3), (4), and (5) Are Longitudinal Gages
 (1.2) and (1.3) Are Transverse Gages
 Gage Location Dimensions Are Shown in Figs. 13 through 16

Cone Half-Angle, θ , deg	Cone Length, L , in.	Cylinder Length, L_{cyl} , in.
2.0	14.04	7.00
5.0	5.61	6.39
7.5	3.73	8.27
10.0	2.79	9.21

Fig. 6 Dimensions of the Solid Cone Specimens

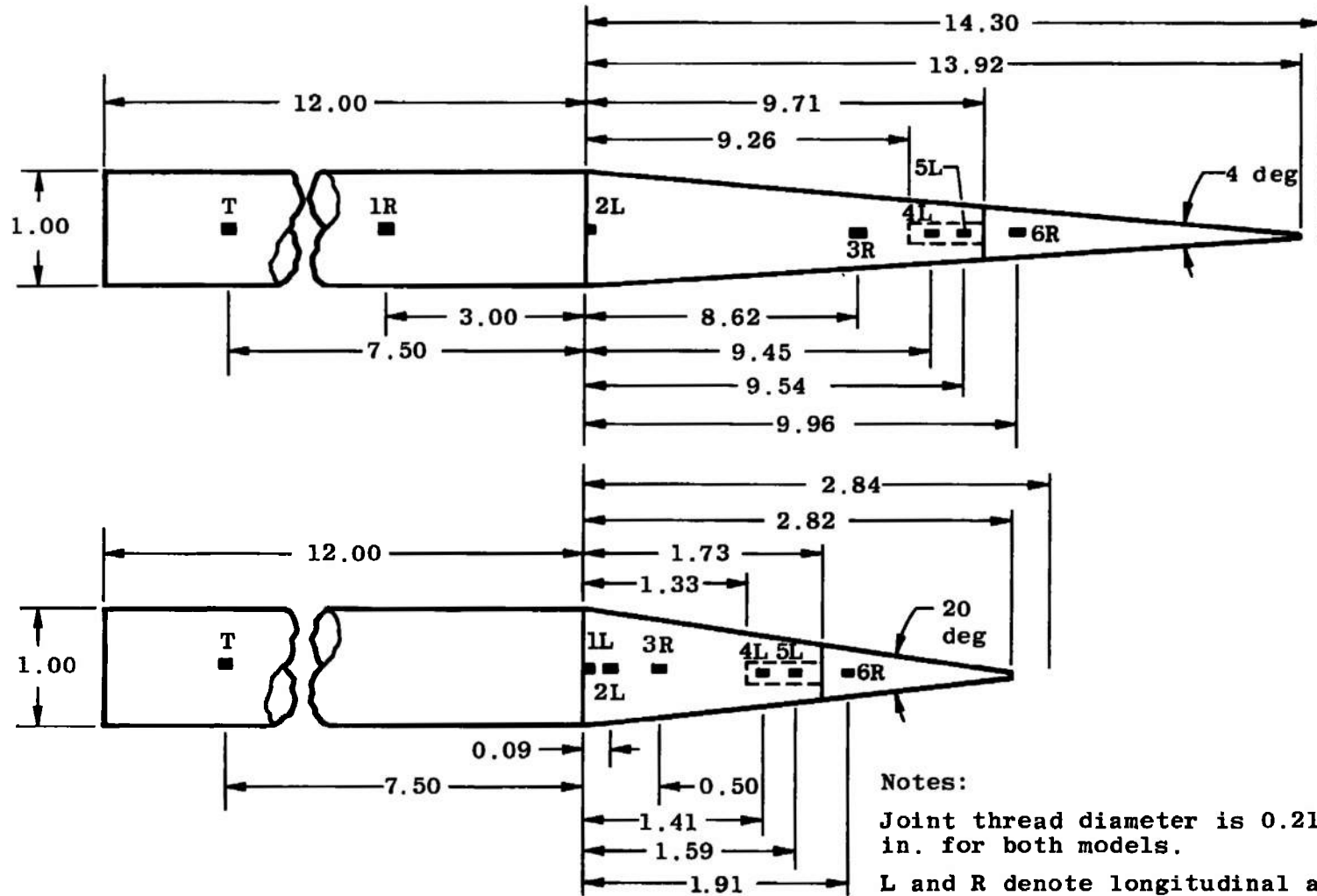


Fig. 7 Jointed Cone Specimen Dimensions and Strain-Gage Locations

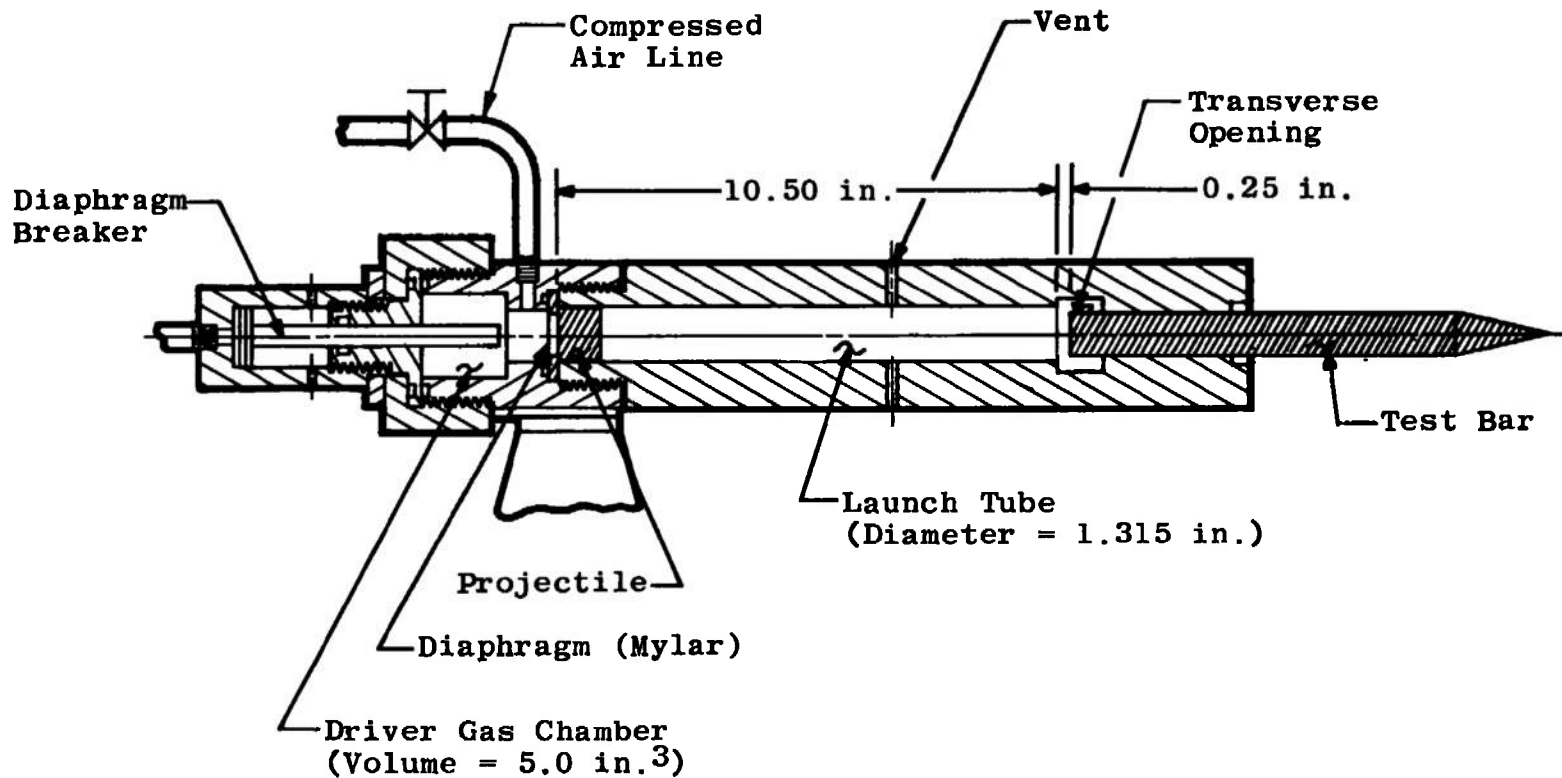


Fig. 8 Section View of Air Gun with Test Bar Installed in Firing Position

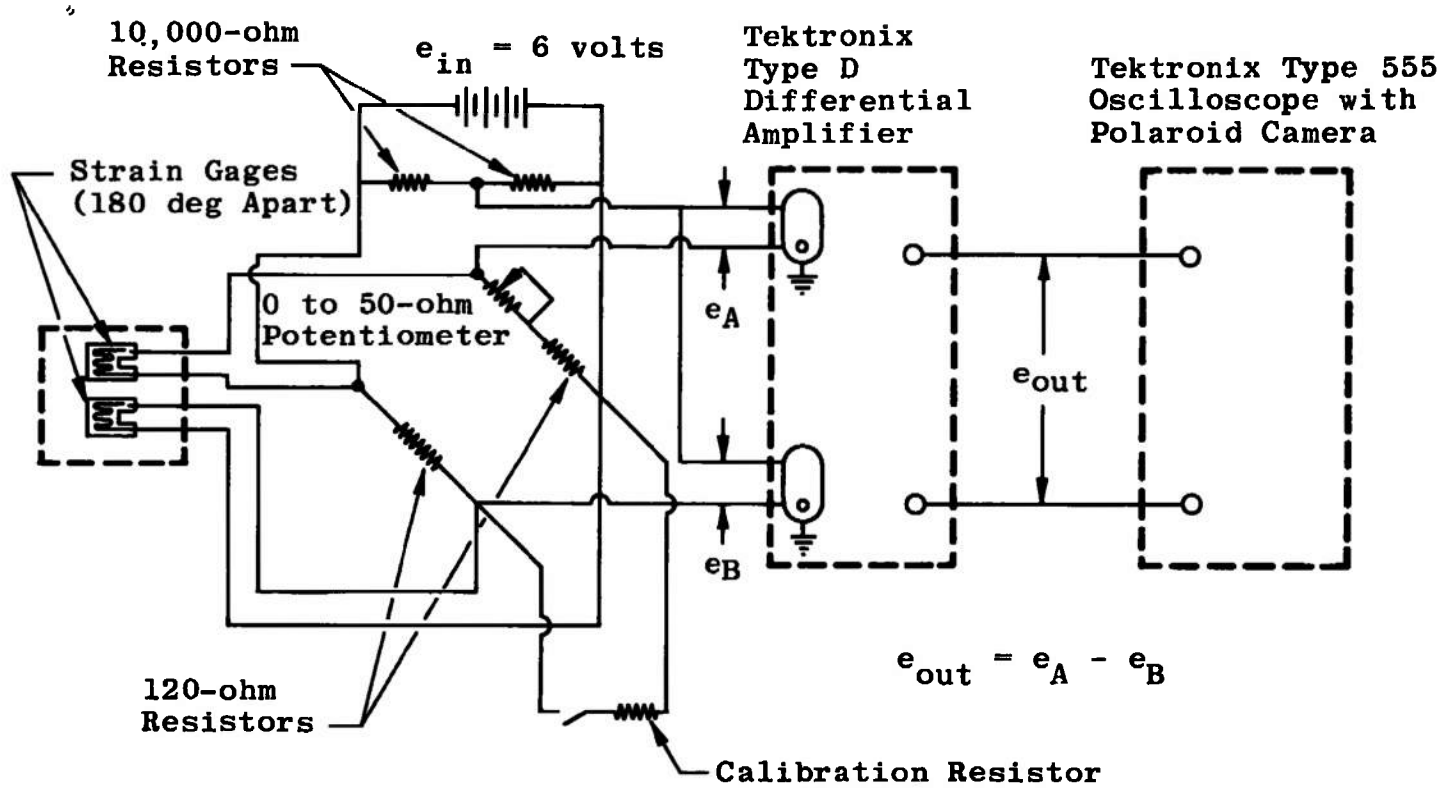
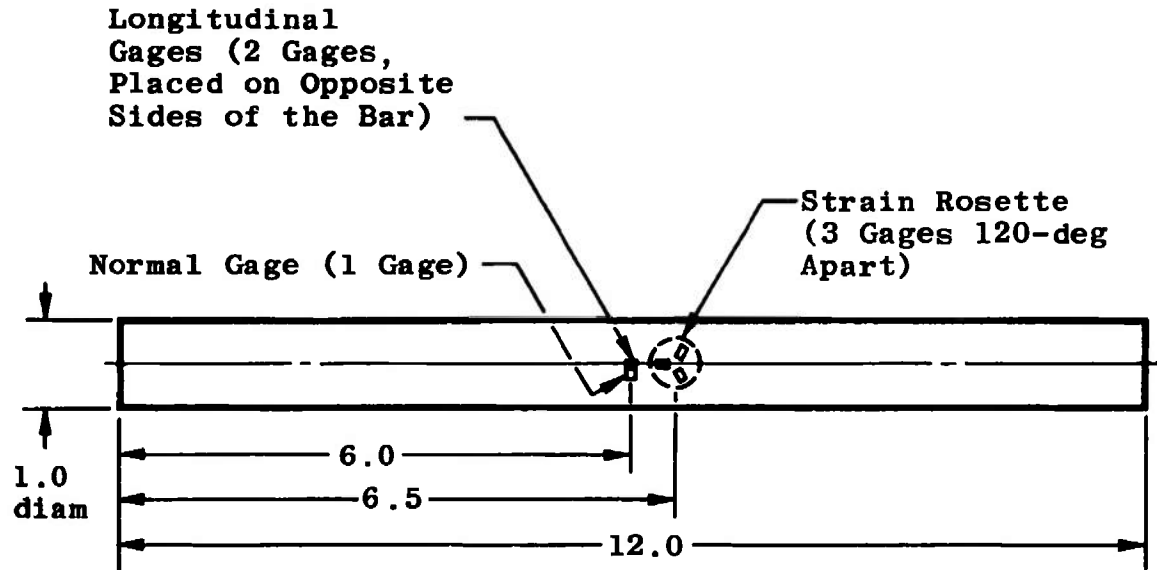


Fig. 9 Typical Bridge Circuit for Measuring and Recording Transient Strains



All Dimensions in Inches

Fig. 10 Detail of Test Cylinder Showing Gauge Location and Orientation

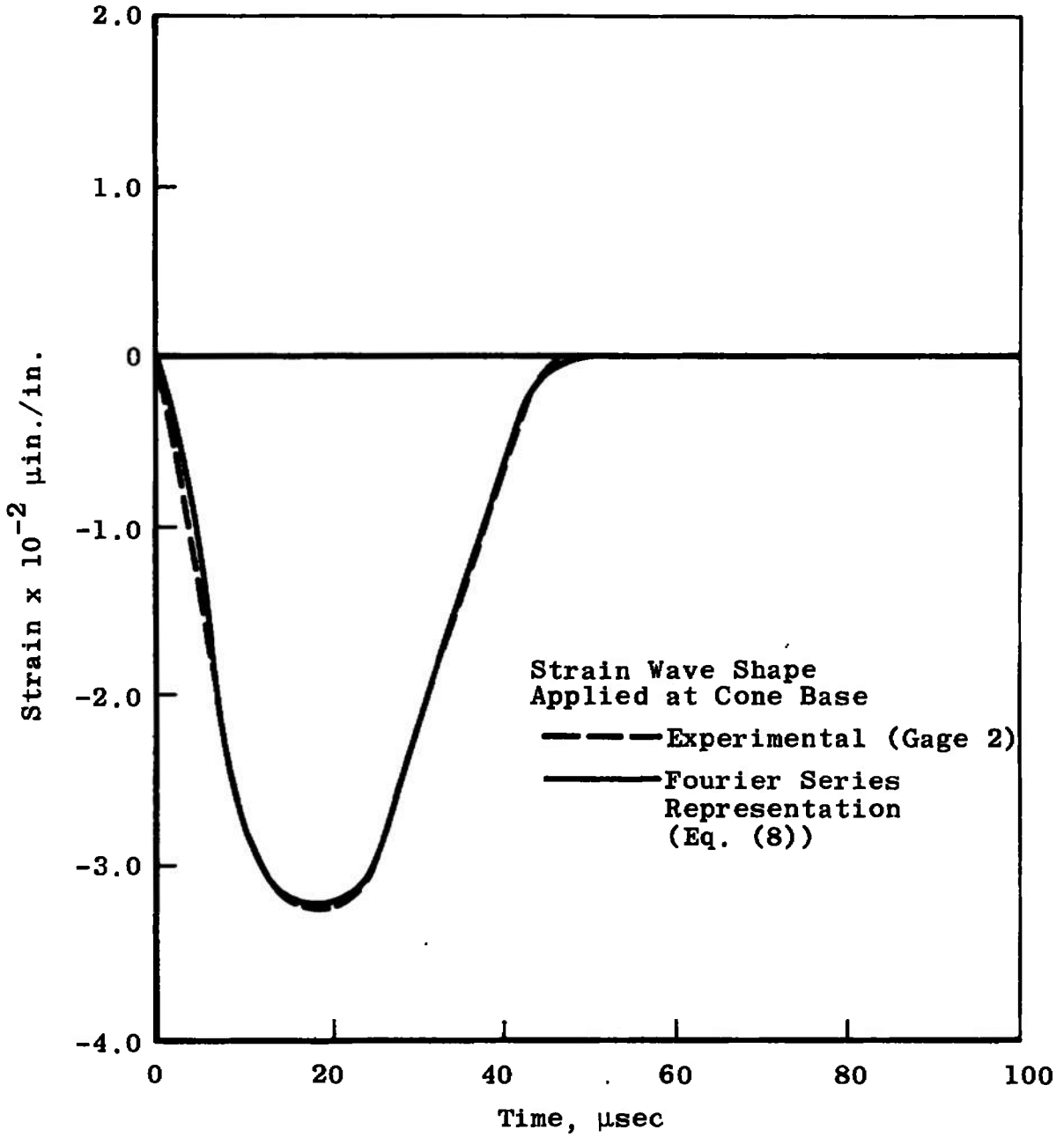


Fig. 11 Strain Pulse Applied to Base of 2-deg Semi-Angle Solid Cone

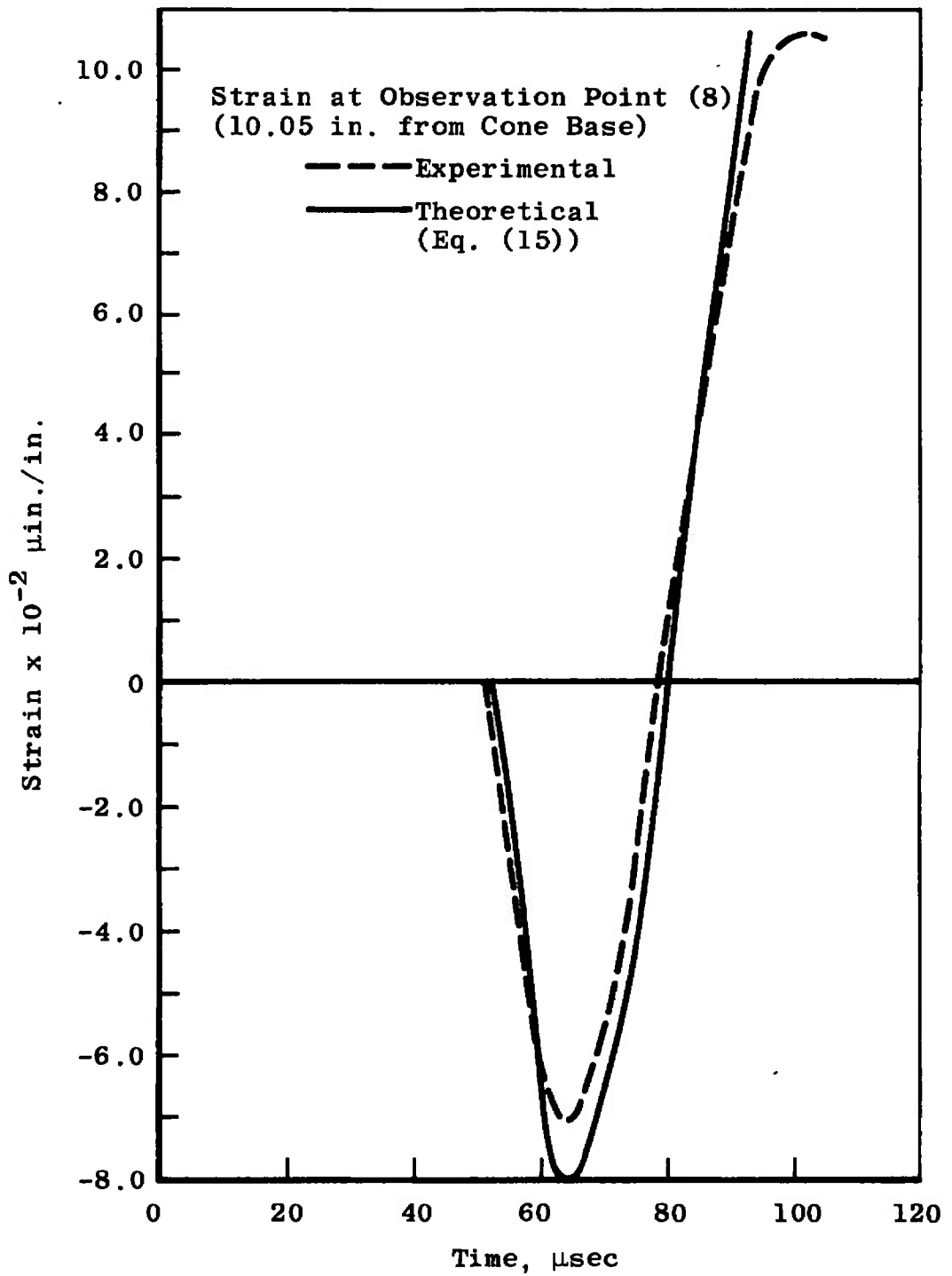


Fig. 12 Experimental and Theoretical Strain at Gage No. 8 (10.05 in. from Cone Base) for 2-deg Semi-Angle Solid Cone

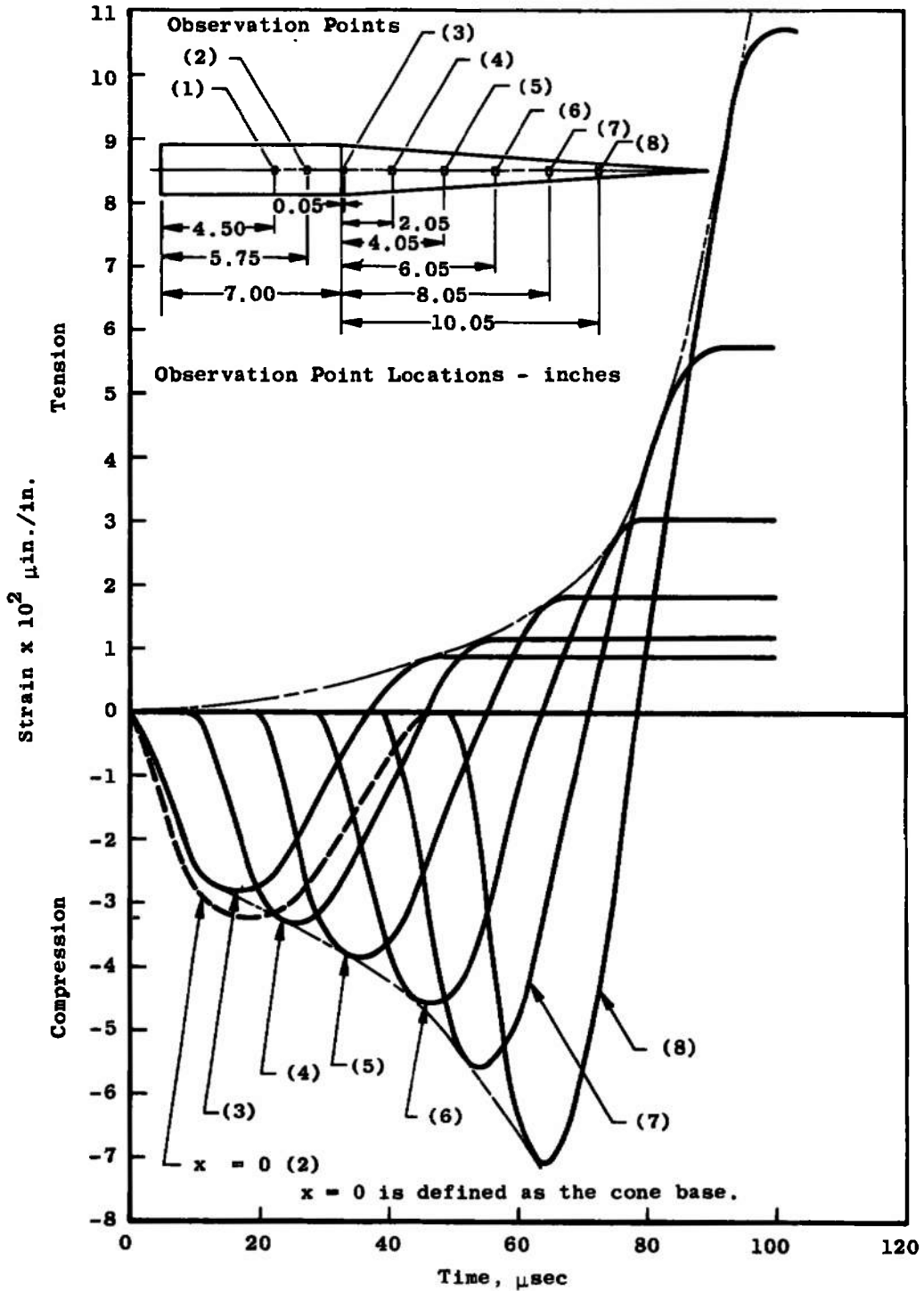


Fig. 13 Longitudinal Strain, as a Function of Time, Measured on the 2-deg Semi-Angle Solid Cone as the Wave Propagated from the Base to the Apex

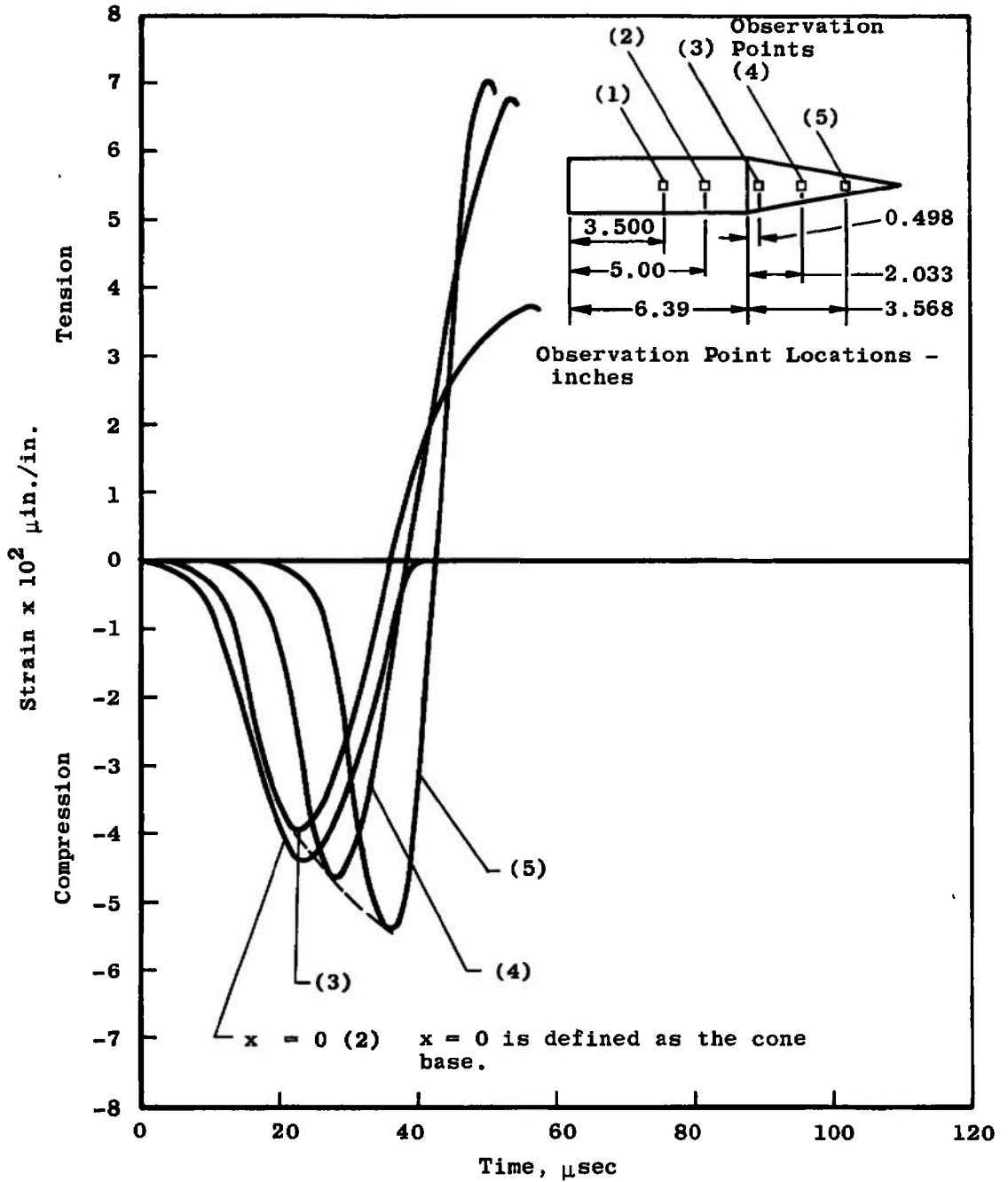


Fig. 14 Longitudinal Strain, as a Function of Time, Measured on the 5-deg Semi-Angle Solid Cone as the Wave Propagated from the Base to the Apex

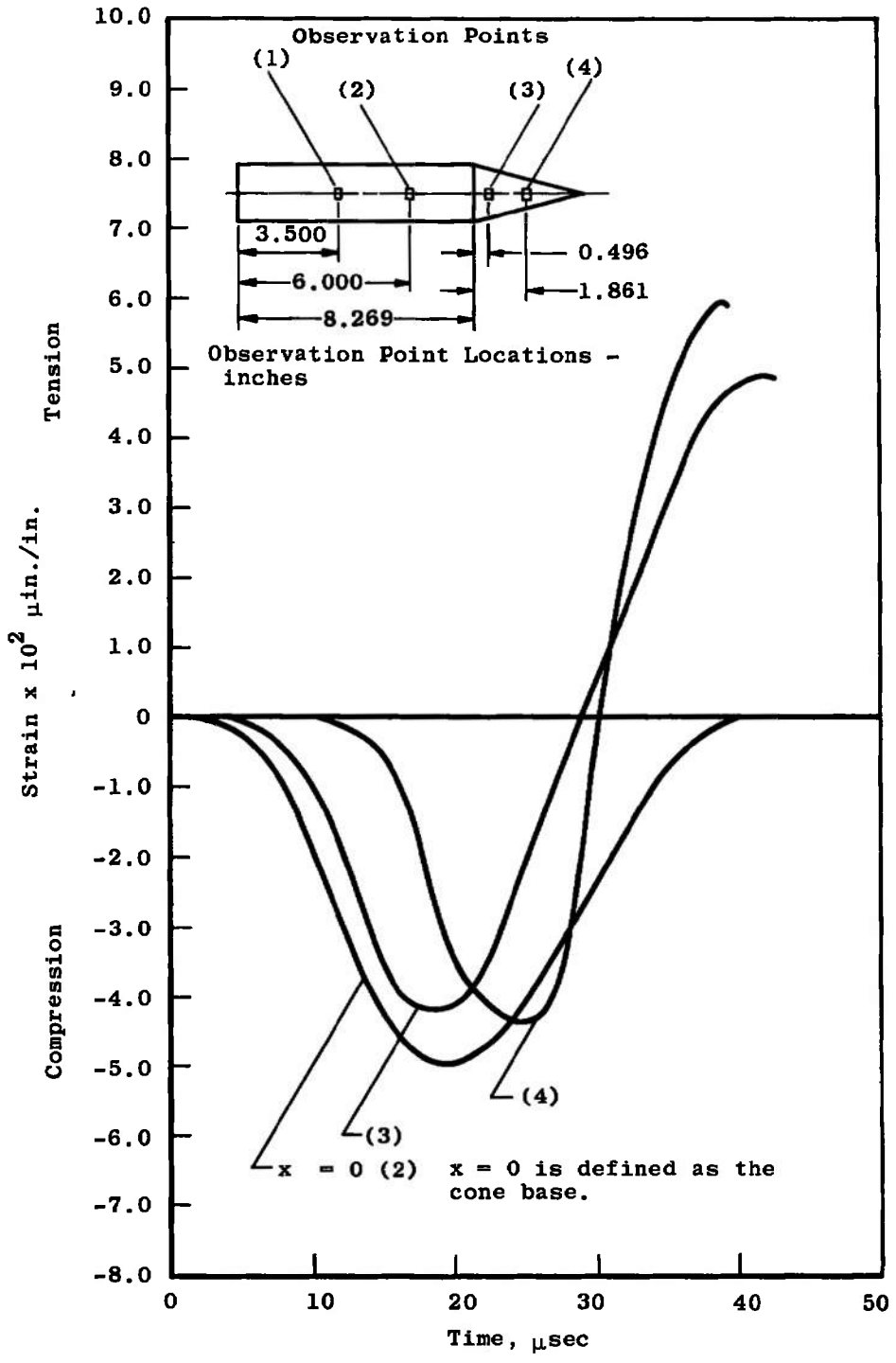


Fig. 15 Longitudinal Strain, as a Function of Time, Measured on the 7.5-deg Semi-Angle Solid Cone as the Wave Propagated from the Base to the Apex

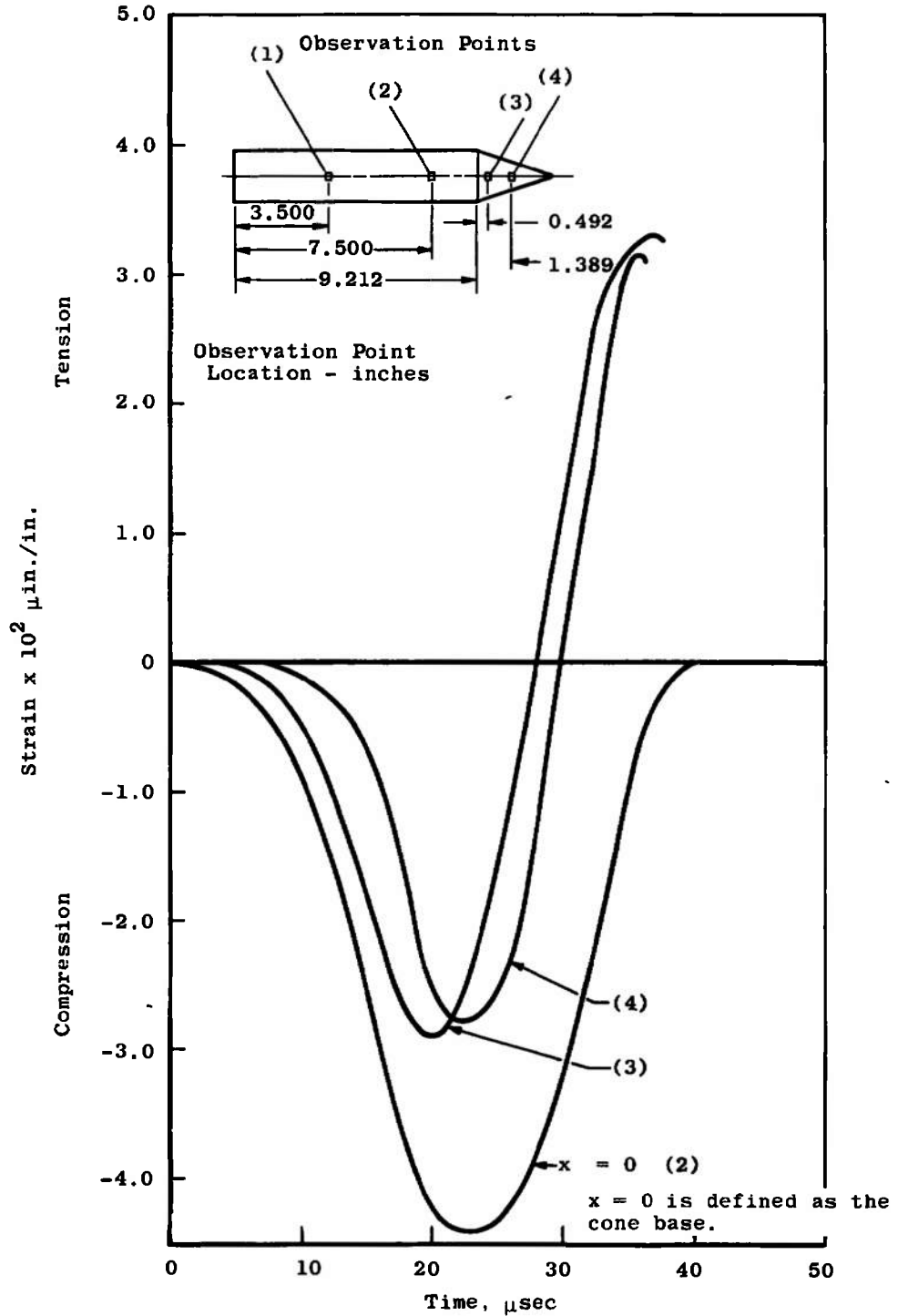


Fig. 16 Longitudinal Strain, as a Function of Time, Measured on the 10-deg Semi-Angle Solid Cone as the Wave Propagated from the Base to the Apex

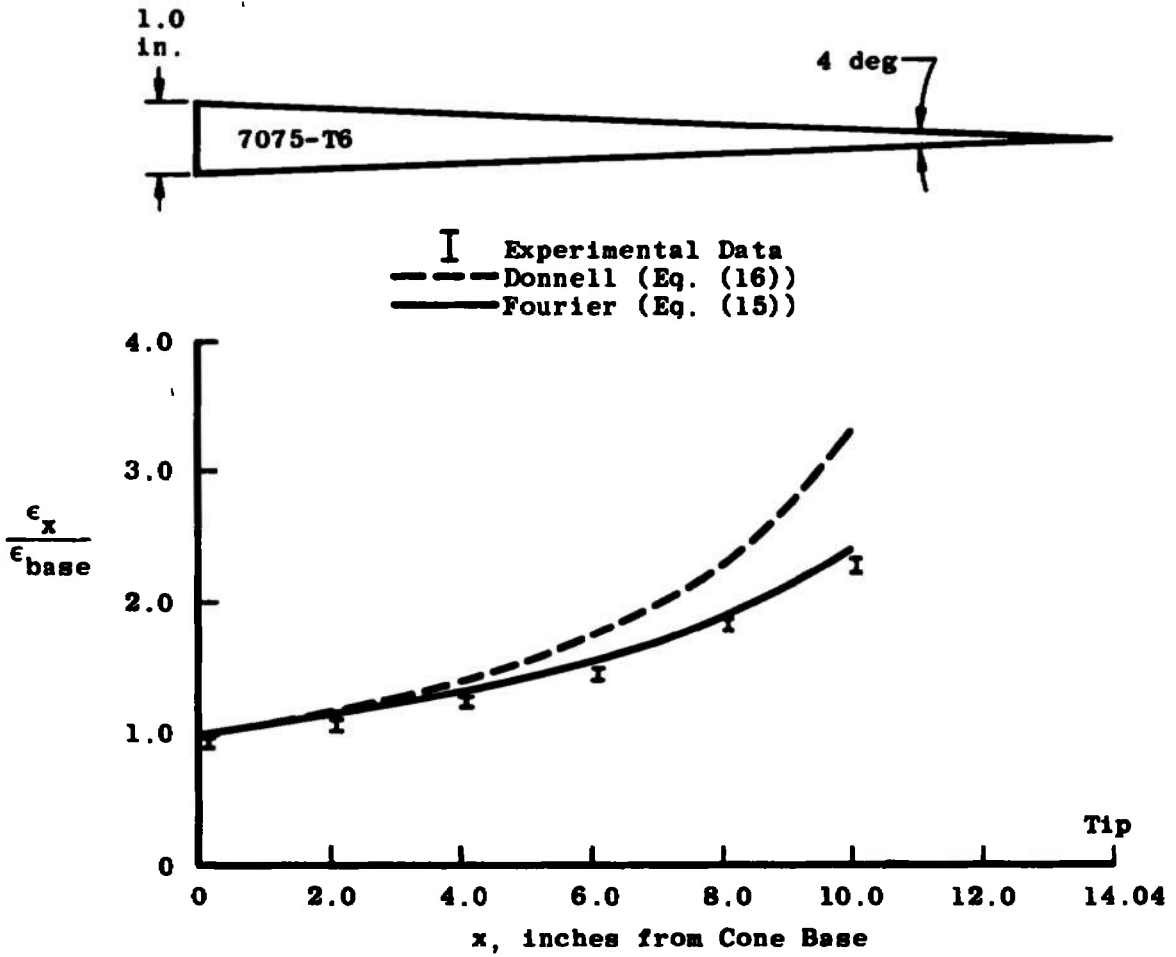


Fig. 17 Comparison of Theoretical with Experimentally Determined Strain Amplification in a 2-deg Semi-Angle Solid Cone

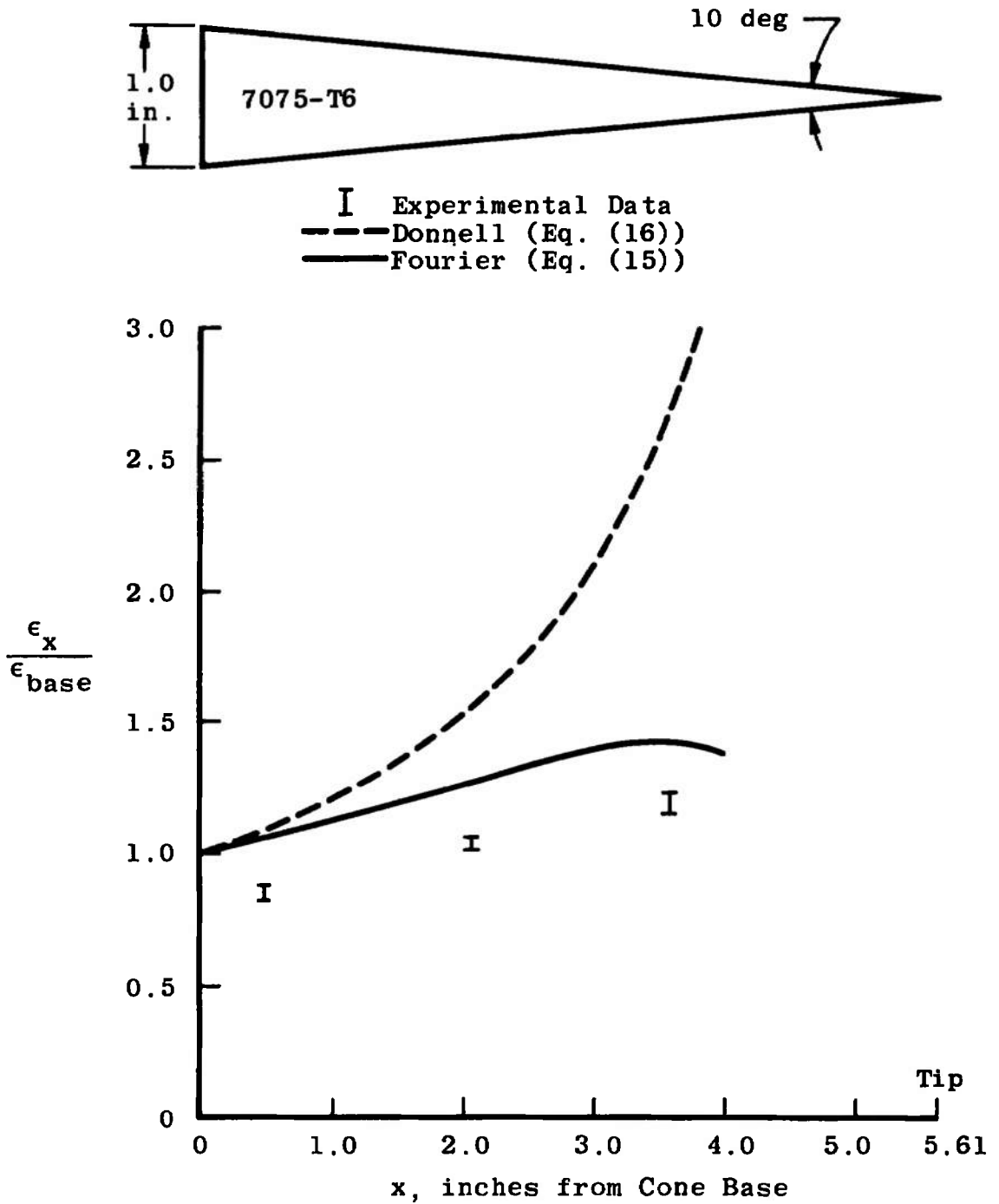


Fig. 18 Comparison of Theoretical with Experimentally Determined Strain Amplification in a 5-deg Semi-Angle Solid Cone

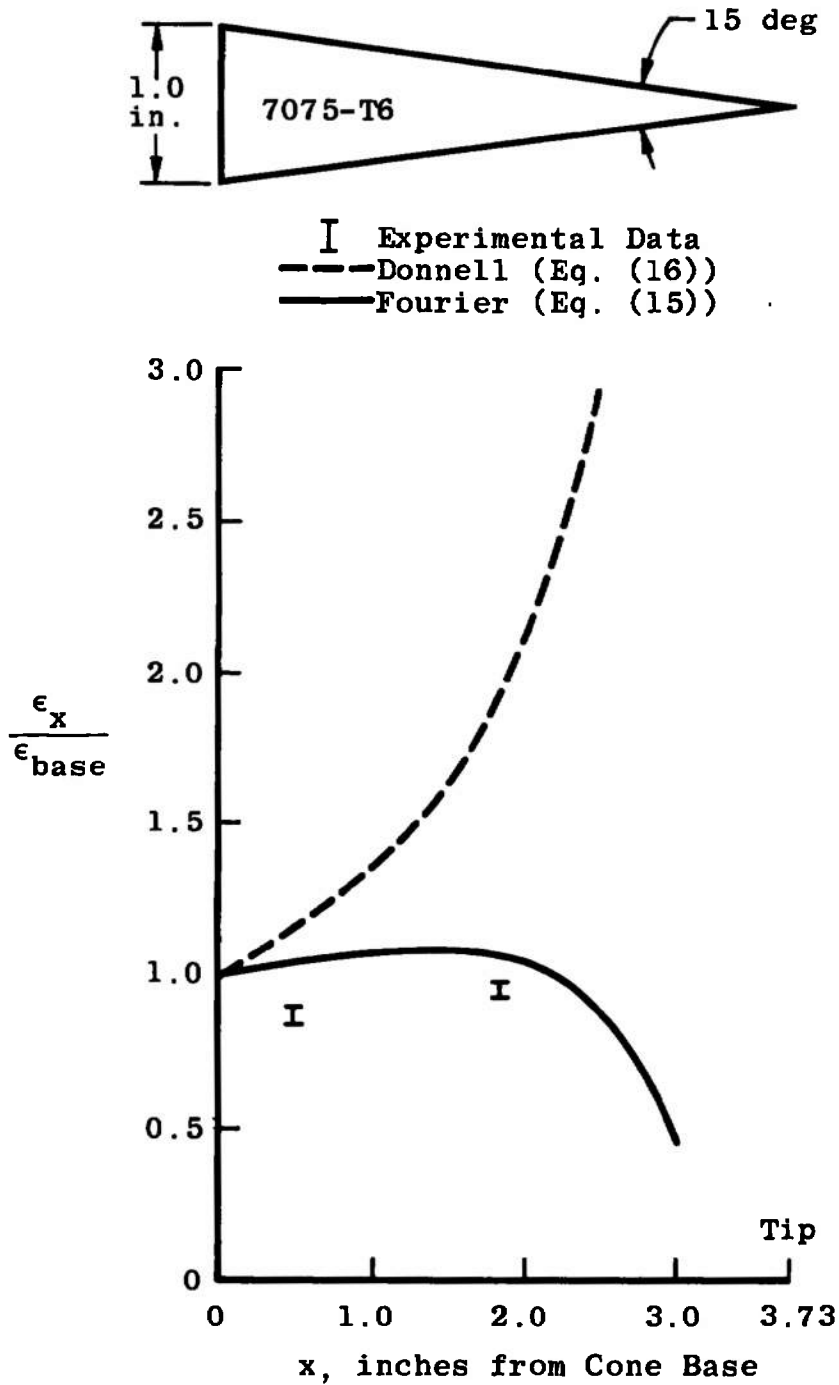


Fig. 19 Comparison of Theoretical with Experimentally Determined Strain Amplification in a 7.5-deg Semi-Angle Solid Cone

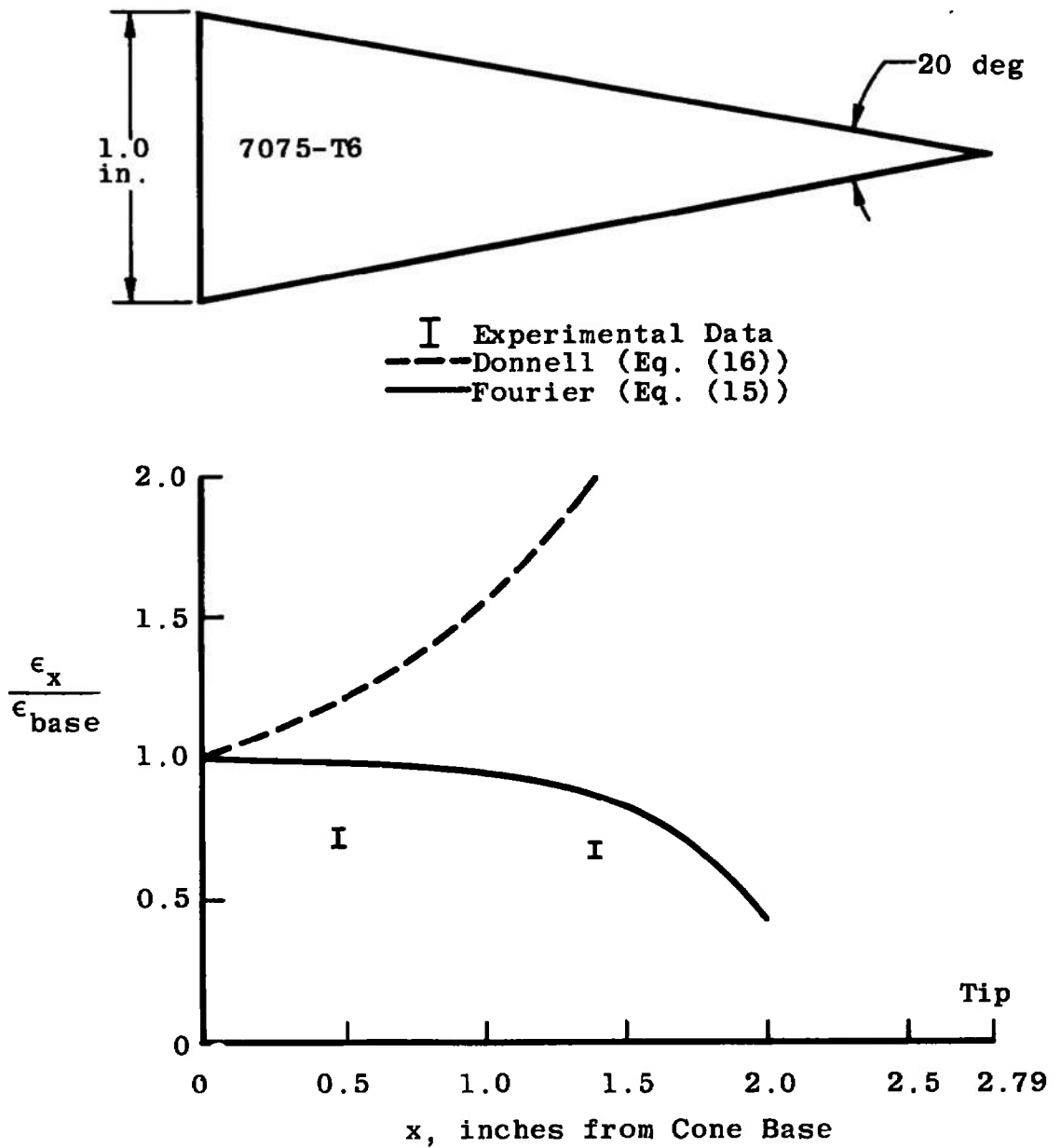


Fig. 20 Comparison of Theoretical with Experimentally Determined Strain Amplification in a 10-deg Semi-Angle Solid Cone

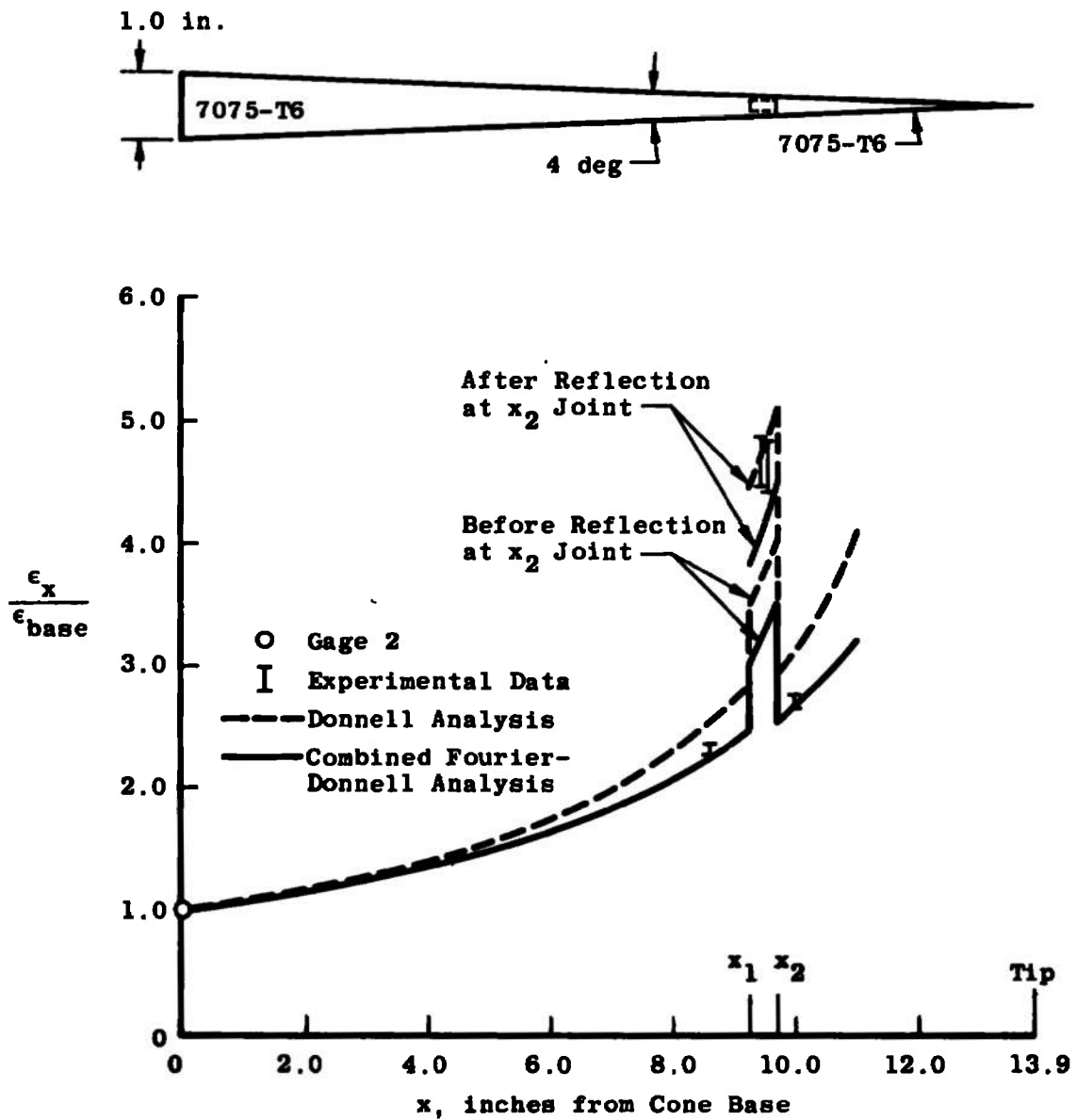


Fig. 21 Theoretical and Experimental Strain Amplification in a Jointed 2-deg Semi-Angle Cone, 90-deg Attachment Angle, 7075-T6 Tip

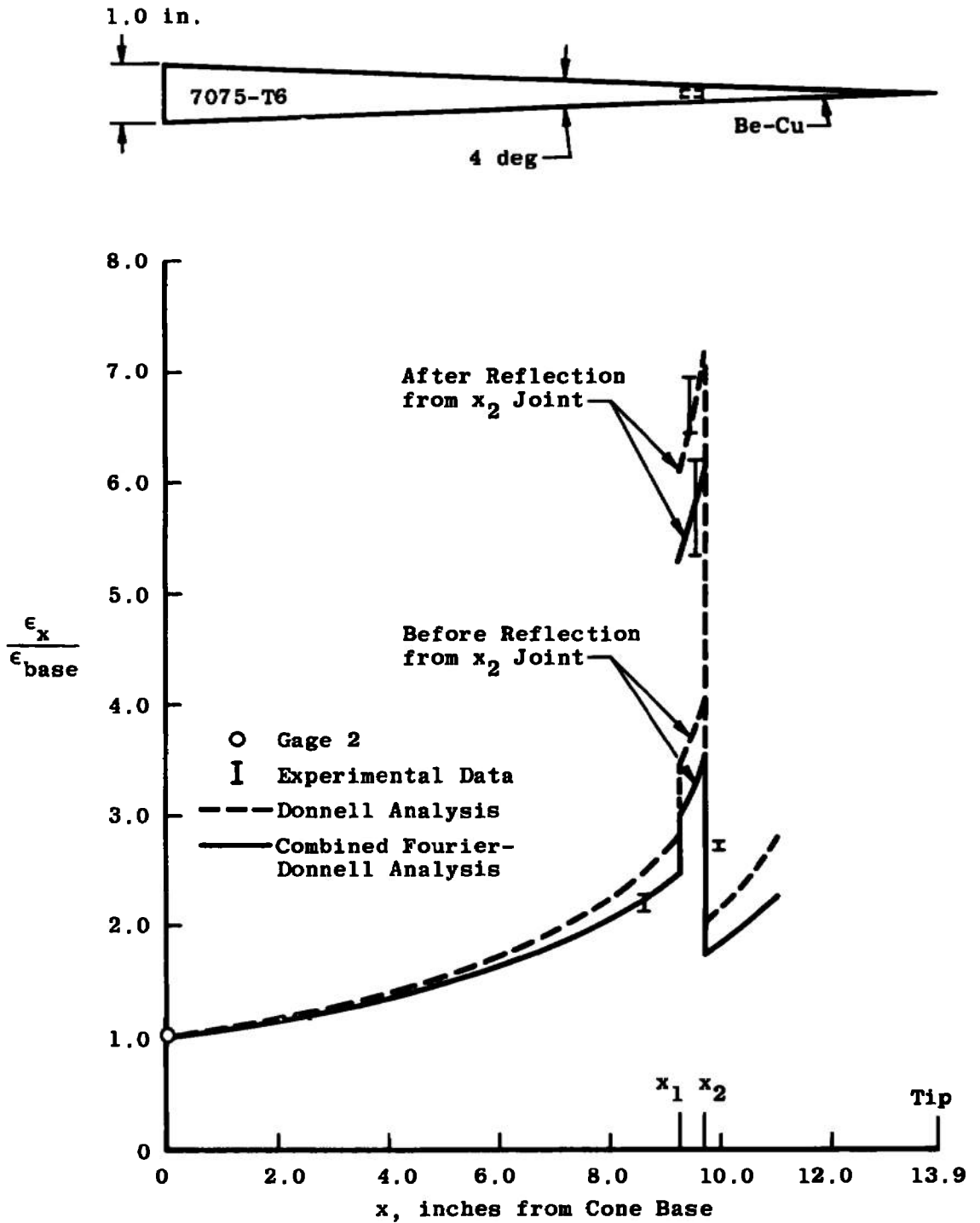


Fig. 22 Theoretical and Experimental Strain Amplification in a Bimetallic 2-deg Semi-Angle Cone, 90-deg Attachment Angle, Beryllium-Copper Tip

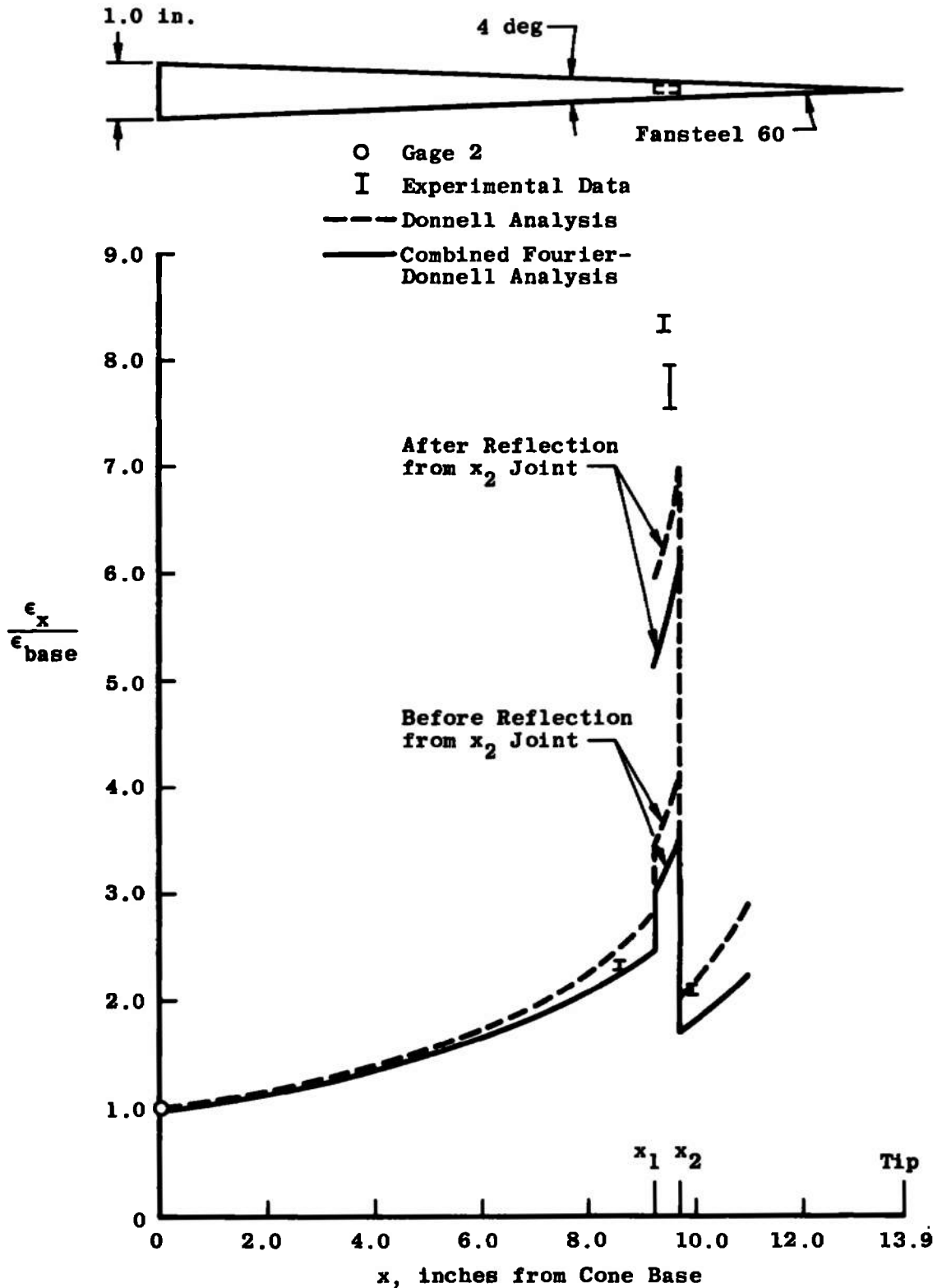


Fig. 23 Theoretical and Experimental Strain Amplification in a Bimetallic 2-deg, Semi-Angle Cone, 90-deg Attachment Angle, Fansteel 60 Tip

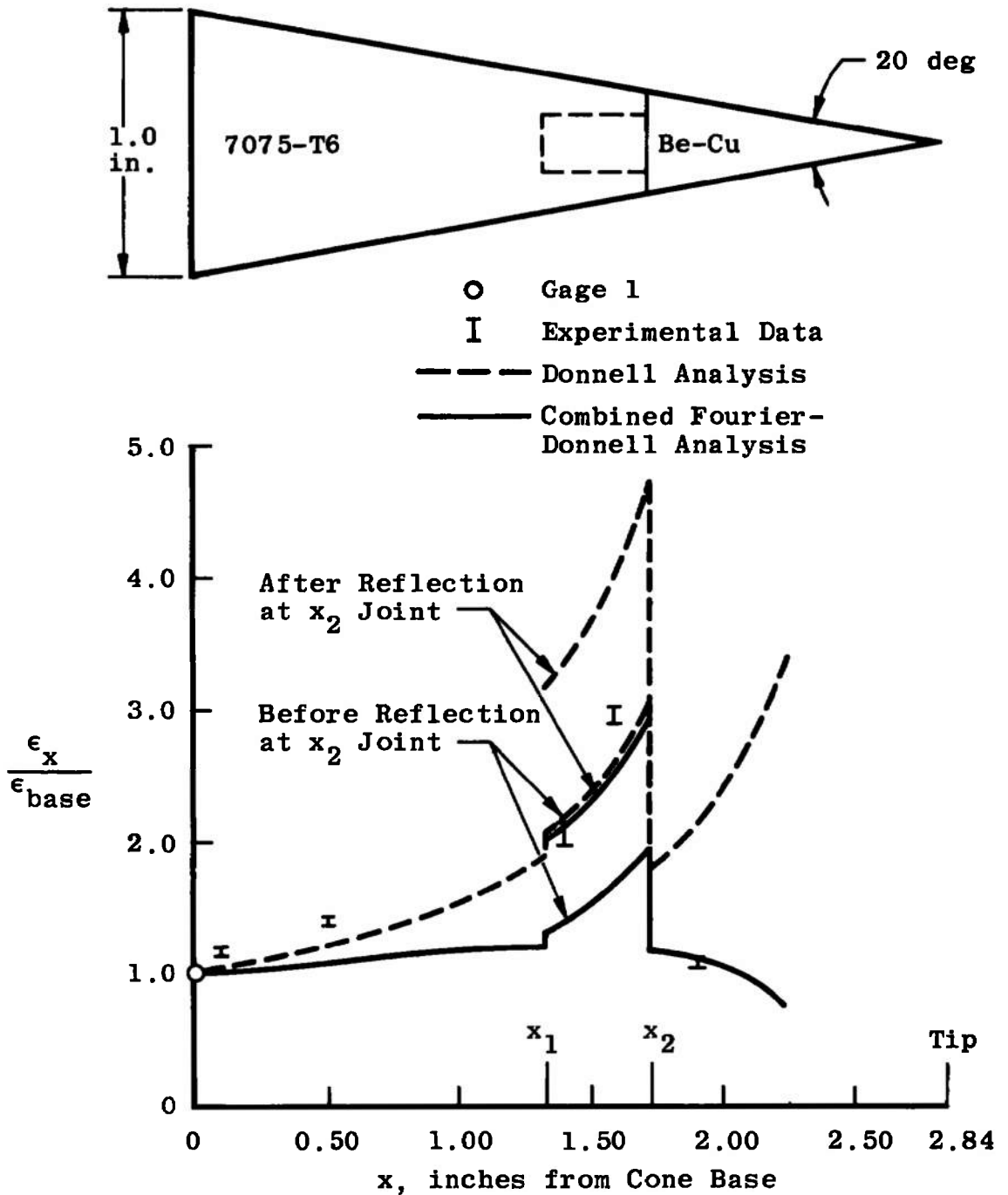


Fig. 24 Theoretical and Experimental Strain Amplification in a Bimetallic 10-deg Semi-Angle Cone, 90-deg Attachment Angle, Beryllium-Copper Tip

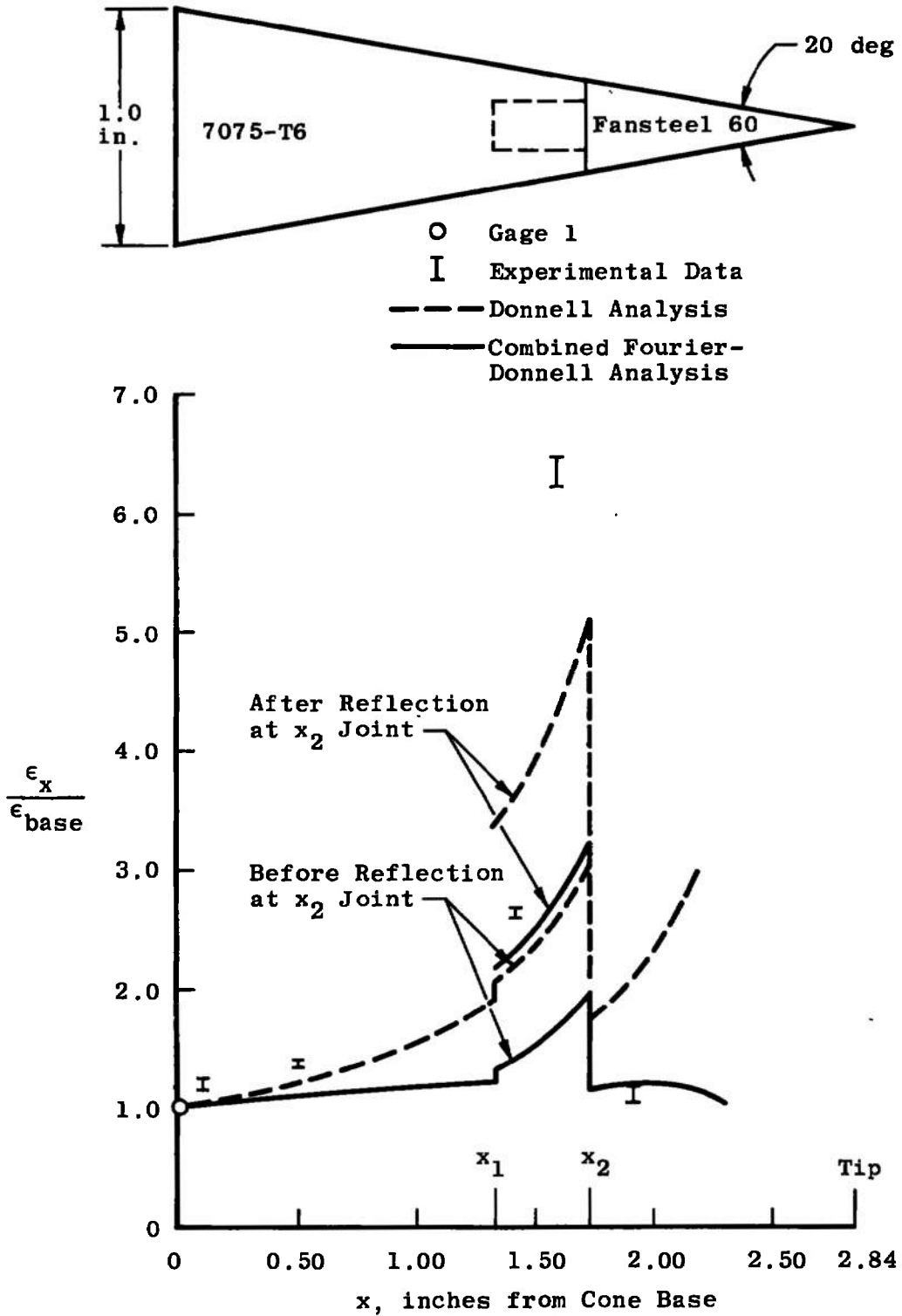


Fig. 25 Theoretical and Experimental Strain Amplification in a Bimetallic 10-deg Semi-Angle Cone, 90-deg Attachment Angle, Fansteel 60 Tip

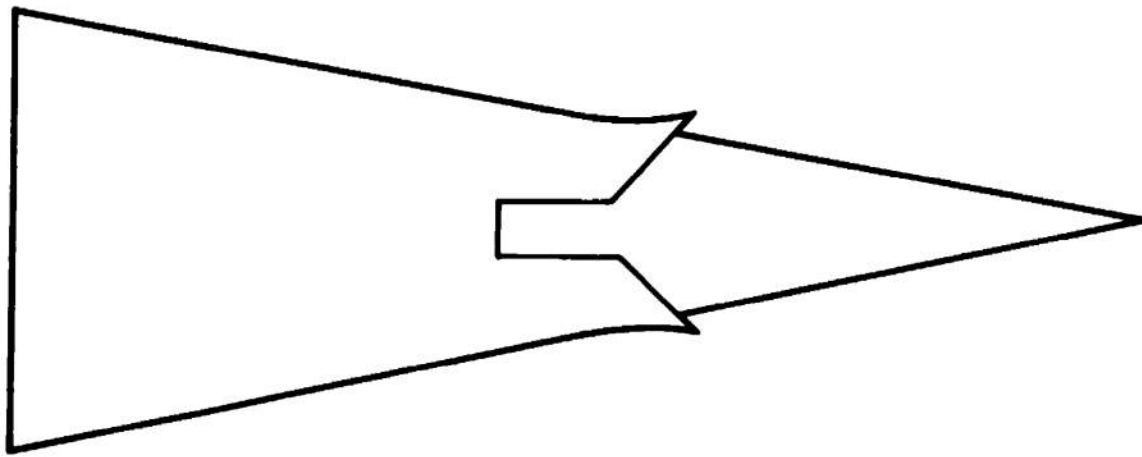


Fig. 26 Typical Permanent Distortion at 45-deg Tip Joint

**TABLE I
MATERIAL PROPERTIES OF SPECIMENS**

Material	W, lb/ft ³	ρ , lb-sec ² /ft ⁴	E x 10 ⁻⁶		\bar{C}	
			lb/in. ²	lb/ft ²	ft/sec	in./ μ sec
7075-T6	174.5	5.42	10.4	1498.0	16600	0.198
Beryllium-Copper	513.0	15.93	19.0	2735.0	13100	0.157
Fansteel 60	1050.0	32.6	21.0	3025.0	9160	0.110

**TABLE II
STRAIN TRANSMISSION AND REFLECTIVITY PARAMETERS AT X₁**

$\theta_{A'}$, deg	A _{A'} , in. ²	A _{B'} , in. ²	r _{AB'} , Eq. (21)	$\frac{\epsilon_{trans}}{\epsilon}$, Eq. (18)	$\frac{\epsilon_{refl}}{\epsilon}$, Eq. (20)
2	0.0975	0.0621	0.637	1.222	-0.222
10	0.2198	0.2198	0.840	1.087	-0.087

**TABLE III
STRAIN TRANSMISSION AND REFLECTIVITY PARAMETERS AT X₂**

Tip Metal	θ , deg	A _{A'} , in. ²	A _{B'} , in. ²	r _{AB'} , Eq. (21)	$\frac{\epsilon_{trans}}{\epsilon}$	$\frac{\epsilon_{refl}}{\epsilon}$
7075-T6	2	0.0455	0.0809	1.778	0.720	0.280
	10	0.0825	0.1178	1.427	0.825	0.175
Be-Cu	2	0.0455	0.0809	4.170	0.497	0.760
	10	0.0825	0.1178	3.345	0.591	0.540
Fansteel 60	2	0.0455	0.0809	5.940	0.477	0.712
	10	0.0825	0.1178	4.770	0.573	0.653

$$r_{AB} = \frac{A_B \rho_B \bar{C}_B}{A_A \rho_A \bar{C}_A} \quad \text{Eq. (21)} \quad \frac{\epsilon_{trans}}{\epsilon} = \left(\frac{2r_{AB}}{r_{AB} + 1} \right) \frac{A_A}{A_B} \frac{E_A}{E_B} \quad \text{Eq. (18)} \quad \frac{\epsilon_{refl}}{\epsilon} = \left(\frac{r_{AB} - 1}{r_{AB} + 1} \right) \quad \text{Eq. (20)}$$

TABLE IV
CROSS-SECTIONAL DIMENSIONS AND AREA RATIOS FOR
SOLID AND JOINTED CONE SPECIMENS

2-deg Semi-Angle Solid and Jointed Cone

x , in.	$d_{x'}$ in.	$A_{x'}$ in. ²	$A_x - A_t$ in. ²	$\left(\frac{A_{base}}{A_x}\right)^{1/2}$	$\left(\frac{A_{x_1} - A_t}{A_x - A_t}\right)^{1/2}$	$\left(\frac{A_{x_2} - A_t}{A_x - A_t}\right)^{1/2}$
0	1.000	0.785	~	1.000	~	~
1.00	0.930	0.879	~	1.076	~	~
3.00	0.790	0.490	~	1.267	~	~
5.00	0.650	0.332	~	1.540	~	~
7.00	0.510	0.205	~	1.960	~	~
9.00	0.370	0.108	~	2.703	~	~
9.26	0.352	0.097	0.062	2.841	1.000	0.656
9.30	0.349	0.096	0.061	2.665	1.013	0.667
9.40	0.343	0.092	0.057	2.915	1.046	0.695
9.50	0.335	0.088	0.053	2.965	1.082	0.927
9.60	0.326	0.085	0.049	3.049	1.121	0.960
9.71	0.321	0.081	0.046	3.115	1.168	1.000
10.00	0.300	0.071	~	3.333	~	~
11.00	0.230	0.042	~	4.346	~	~
12.00	0.161	0.020	~	6.211	~	~

5-deg Semi-Angle Cone

x , in.	$d_{x'}$ in.	$\left(\frac{A_{base}}{A_x}\right)^{1/2}$
0	0.500	1.000
1.0	0.413	1.212
2.0	0.325	1.538
3.0	0.238	2.105
4.0	0.150	3.333
5.0	0.063	8.000

10-deg Semi-Angle Solid and Jointed Cone

0	1.000	0.785	~	1.000	~	~
0.500	0.624	0.533	~	1.214	~	~
0.750	0.735	0.425	~	1.360	~	~
1.000	0.647	0.329	~	1.545	~	~
1.340	0.529	0.220	0.165	1.890	1.000	0.669
1.400	0.506	0.201	0.166	1.976	1.054	0.705
1.500	0.471	0.174	0.139	2.123	1.153	0.771
1.600	0.436	0.149	0.114	2.294	1.274	0.651
1.740	0.367	0.118	0.083	2.584	1.497	1.000
1.900	0.330	0.085	~	3.030	~	~
2.000	0.295	0.068	~	3.390	~	~
2.250	0.208	0.033	~	4.854	~	~

7.5-deg Semi-Angle Solid Cone

0	0.500	1.000
1.0	0.388	1.358
2.0	0.237	2.112
2.5	0.171	2.926
3.0	0.105	4.781

See
Eq. (16)

$d_t = 0.212$ in.
 $A_t = 0.035$ in.²

See
Eq. (16)

TABLE V
STRAIN AMPLIFICATION FACTORS FROM DONNELL'S ANALYSIS
FOR 2-DEG SEMI-ANGLE CONES

x	$\epsilon_x / \epsilon_{\text{base}}$					
	7075-T6	Tip	Be-Cu	Tip	Fansteel 60	Tip
0	1.00		1.00		1.00	
1.00	1.08		1.08		1.08	
3.00	1.27		1.27		1.27	
5.00	1.54		1.54		1.54	
7.00	1.96		1.96		1.96	
9.00	2.70		2.70		2.70	
9.26	2.85		2.85		2.85	
9.26	3.48	↓ After Strain Reflection at x ₂	3.48	↓ After Strain Reflection at x ₂	3.48	↓ After Strain Reflection at x ₂
9.30	3.52	4.45	3.52	6.12	3.52	5.95
9.40	3.64	4.51	3.64	6.20	3.64	6.03
9.50	3.76	4.65	3.76	6.40	3.76	6.22
9.60	3.90	4.82	3.90	6.62	3.90	6.44
9.71	4.06	4.94	4.06	6.86	4.06	6.67
9.71	4.06	5.20	4.06	7.15	4.06	6.95
9.71	2.92		2.02		1.94	
10.00	3.12		2.15		2.07	
11.00	4.07		2.81		2.70	
12.00	5.85		4.04		3.87	

TABLE VI
STRAIN AMPLIFICATION FACTORS FROM DONNELL'S ANALYSIS
FOR 10-DEG SEMI-ANGLE CONES

x	$\epsilon_x / \epsilon_{\text{base}}$							
	7075-T6	Tip	Be-Cu	Tip	Fansteel 60	Tip		
0	1.00	After Reflected ↓ Strain at x_2	1.00	After Reflected ↓ Strain at x_2	1.00	After Reflected ↓ Strain at x_2		
0.50	1.21		1.21		1.21			
0.75	1.36		1.36		1.36			
1.00	1.55		1.55		1.55			
1.34	1.89		1.89		1.89			
1.34	2.05		2.41		3.17		2.05	3.40
1.40	2.17		2.55		3.33		2.17	3.58
1.50	2.37		2.78		3.65		2.37	3.92
1.60	2.62		3.08		4.03		2.62	4.33
1.74	3.08		3.62		4.74		3.08	5.09
1.74	2.54				1.82		1.76	
1.90	2.98				2.13		2.07	
2.00	3.34				2.30		2.32	
2.25	4.76				3.41		3.31	

TABLE VII
STRAIN AMPLIFICATION FACTORS FROM THE COMBINED
FOURIER-DONNELL ANALYSIS FOR 2-DEG SEMI-ANGLE CONES

x	$\epsilon_x / \epsilon_{\text{base}}$								
	7075-T6	Tip	Be-Cu	Tip	Fansteel 60	Tip			
0	1.00	After Reflected ↓ Strain from x2	1.00	After Reflected ↓ Strain from x2	1.00	After Reflected ↓ Strain from x2			
3.00	1.24		1.24		1.24				
6.60	1.63		1.63		1.63				
8.62	2.23		2.23		2.23				
9.26	2.45		2.45		2.45				
9.26	3.00		3.84		3.00		5.29	3.00	5.15
9.30	3.04		3.89		3.04		5.36	3.04	5.21
9.40	3.14		4.02		3.14		5.53	3.14	5.38
9.50	3.25		4.16		3.25		5.72	3.25	5.68
9.60	3.36		4.31		3.36		5.93	3.36	5.77
9.71	3.52		4.51		3.52		6.20	3.52	6.03
9.71	2.54				1.75			1.68	
9.96	2.65				1.83			1.77	
10.46	2.89				2.02			1.96	
11.00	3.19				2.25			2.22	
12.00	3.90				2.85			2.93	

TABLE VIII
STRAIN AMPLIFICATION FACTORS FROM THE COMBINED
FOURIER-DONNELL ANALYSIS FOR 10-DEG SEMI-ANGLE CONES

x	$\epsilon_x / \epsilon_{\text{base}}$							
	7075-T6	Tip	Be-Cu	Tip	Fansteel 60	Tip		
0	1.00	After Reflected ↓ Strain from x2	1.00	After Reflected ↓ Strain from x2	1.00	After Reflected ↓ Strain from x2		
0.09	1.02		1.02		1.02			
0.50	1.09		1.09		1.09			
1.00	1.18		1.18		1.18			
1.33	1.21		1.21		1.21			
1.33	1.32		1.55		2.03		1.32	2.18
1.40	1.39		1.63		2.14		1.39	2.29
1.60	1.68		1.97		2.58		1.68	2.77
1.73	1.97		2.31		3.03		1.97	3.23
1.73	1.62				1.16		1.13	
1.83	1.52				1.16		1.15	
1.91	1.42				1.14		1.18	
2.03	1.19				1.05		1.20	
2.23	0.65				0.76		1.12	

UNCLASSIFIED

Security Classification

DOCUMENT CONTROL DATA - R & D

(Security classification of title, body of abstract and indexing annotation must be entered when the overall report is classified)

1 ORIGINATING ACTIVITY (Corporate author) Arnold Engineering Development Center Arnold Air Force Station, Tennessee 37389	2a. REPORT SECURITY CLASSIFICATION UNCLASSIFIED 2b. GROUP N/A
---	---

3 REPORT TITLE
AN INVESTIGATION OF STRAIN WAVE PROPAGATION IN METALLIC CONICAL RODS

4 DESCRIPTIVE NOTES (Type of report and inclusive dates)
Final Report - January 1968 to July 1972

5 AUTHOR(S) (First name, middle initial, last name)
J. P. Billingsley, P. A. Evans, and R. L. Nenninger, ARO, Inc.

6 REPORT DATE June 1973	7a. TOTAL NO. OF PAGES 69	7b. NO OF REFS 18
-----------------------------------	-------------------------------------	-----------------------------

6a. CONTRACT OR GRANT NO b. PROJECT NO c. Program Element 65802F d	9a. ORIGINATOR'S REPORT NUMBER(S) AEDC-TR-73-94 9b. OTHER REPORT NO(S) (Any other numbers that may be assigned this report) ARO-VKF-TR-73-41
--	---

10 DISTRIBUTION STATEMENT
Approved for public release; distribution unlimited.

11 SUPPLEMENTARY NOTES Available in DDC	12 SPONSORING MILITARY ACTIVITY Arnold Engineering Development Center, Air Force Systems Command, Arnold AF Station, Tennessee 37389
---	--

13. ABSTRACT
Strain wave propagation in metal cones with a compressive pulse applied at the base has been investigated experimentally and theoretically. This study was motivated by the need for design information for gun-launched models used in aerophysics research. The results are also directly applicable to the design of ordinary gun-launched munitions or to any other cases of impulsive loading on conical bars. The effect of the following parameters was considered: (1) cone angle, (2) cone tip joint (threaded connection), and (3) cone tip material variation (7075-T6 base with 7075-T6, beryllium-copper, and Fansteel 60 tips). Transient strains were measured with strain gages mounted at critical locations on the specimen. It was found that increasing the cone half-angle from 2 to 10 deg reduced the level of strain amplification for both solid and jointed cones. The effect of a threaded junction between the model base and the tip is to increase the strain (or stress) level in the exterior section because of (1) cross-sectional area decrease at the bottom of the threaded hole and (2) reflected strain from the visible tip junction. Tips of heavier, denser material than the base further intensified the strain in the exterior threaded section because of greatly increased strain reflection at the forward junction. The measured strain amplification at the cone surface was compared with predictions based on one-dimensional strain propagation theory. In general, the theoretical predictions were good enough for use (with reasonable discretion) in model designs.

UNCLASSIFIED

Security Classification

14. KEY WORDS	LINK A		LINK B		LINK C	
	ROLE	WT	ROLE	WT	ROLE	WT
strain rates stress analysis wave propagation conical bodies light gas guns						

AFPC
Avionics AFPC Team

UNCLASSIFIED

Security Classification